Cell

Article

A Qrr Noncoding RNA Deploys Four Different Regulatory Mechanisms to Optimize Quorum-Sensing Dynamics

Lihui Feng,[1] Steven T. Rutherford,[1,4] Kai Papenfort,[1] John D. Bagert,[3] Julia C. van Kessel,[1,5] David A. Tirrell,[3] Ned S. Wingreen,[1,*] and Bonnie L. Bassler[1,2,*]

[1]Department of Molecular Biology, Princeton University, Princeton, NJ 08544, USA

[2]Howard Hughes Medical Institute, Chevy Chase, MD 20815, USA

[3]Division of Chemistry and Chemical Engineering, California Institute of Technology, Pasadena, CA 91125, USA

[4]Present address: Genentech, San Francisco, CA 94080, USA

[5]Present address: Department of Molecular and Cellular Biochemistry, Indiana University, Bloomington, IN 47405, USA

*Correspondence: wingreen@princeton.edu (N.S.W.), bbassler@princeton.edu (B.L.B.)

http://dx.doi.org/10.1016/j.cell.2014.11.051

SUMMARY

Quorum sensing is a cell-cell communication process that bacteria use to transition between individual and social lifestyles. In vibrios, homologous small RNAs called the Qrr sRNAs function at the center of quorum-sensing pathways. The Qrr sRNAs regulate multiple mRNA targets including those encoding the quorum-sensing regulatory components *luxR*, *luxO*, *luxM*, and *aphA*. We show that a representative Qrr, Qrr3, uses four distinct mechanisms to control its particular targets: the Qrr3 sRNA represses *luxR* through catalytic degradation, represses *luxM* through coupled degradation, represses *luxO* through sequestration, and activates *aphA* by revealing the ribosome binding site while the sRNA itself is degraded. Qrr3 forms different base-pairing interactions with each mRNA target, and the particular pairing strategy determines which regulatory mechanism occurs. Combined mathematical modeling and experiments show that the specific Qrr regulatory mechanism employed governs the potency, dynamics, and competition of target mRNA regulation, which in turn, defines the overall quorum-sensing response.

INTRODUCTION

Small regulatory RNAs (sRNAs) act as core regulators in many bacterial signal transduction cascades (Waters and Storz, 2009). Bacterial sRNAs function by several mechanisms. Here, we focus on *trans*-encoded Hfq-binding sRNAs. This class of sRNAs can act positively or negatively, and noncontiguous base-pairing with mRNA targets is employed. In the case of negative regulation, *trans*-encoded sRNAs base pair near the ribosome binding site of the mRNA target, leading to ribosome occlusion (Altuvia et al., 1998; Kawamoto et al., 2006; Møller et al., 2002; Udekwu et al., 2005). In most cases, occlusion is associated with RNase E recruitment and degradation of the mRNA (Massé et al., 2003; Prévost et al., 2011). In the case of positive regulation, *trans*-encoded sRNAs perform anti-anti-sense base-pairing with the mRNA target (Fröhlich and Vogel, 2009; Majdalani et al., 1998). Binding reveals the ribosome binding site and promotes stabilization of the mRNA target and, in turn, gene expression (McCullen et al., 2010). The RNA chaperone Hfq mediates the interactions between *trans*-encoded sRNAs and their mRNA targets and protects the sRNAs from RNase E-mediated degradation (Vogel and Luisi, 2011; Kawamoto et al., 2006). Hfq is thought to be limiting, leading to competition between different sRNA-mRNA pairs for its chaperone function (Fender et al., 2010; Hussein and Lim, 2011; Moon and Gottesman, 2011).

The implications of *trans*-encoded sRNA regulation at the systems level depend on the fate of the sRNA. First, sRNAs can undergo coupled degradation in which both the sRNA and the mRNA target are degraded following base-pairing. The RyhB sRNA exemplifies this mode of regulation (Massé et al., 2003). Second, sRNAs can act catalytically, in which the target mRNA is degraded but the sRNA is not. Thus, the sRNA is available to be recycled. One such example is the MicM (ChiX) sRNA, which acts catalytically on the mRNA target *ybfM* (*chiP*) (Overgaard et al., 2009). Third, sRNAs can also act by sequestering their targets. An example of this type of regulation occurs between the sRNA Spot42 and its mRNA target *galK*. In this case, Spot42 specifically blocks the ribosome binding site of *galK*, but no mRNA degradation occurs (Møller et al., 2002). Finally, the fates of sRNAs that act as activators have not been well characterized. In theory, activating sRNAs can be degraded, recycled, or sequestered.

The quorum regulatory RNAs (Qrr) sRNAs are Hfq-dependent *trans*-encoded sRNAs that control vibrio quorum sensing (Lenz et al., 2004). Quorum sensing is a cell-cell communication process that bacteria use to monitor changes in cell-population density and control collective behaviors such as biofilm formation and virulence factor production. Quorum sensing involves production, detection, and population-wide response to extracellular signal molecules called autoinducers (Rutherford and Bassler, 2012). In vibrio quorum-sensing circuits, several nearly identical Qrr sRNAs control multiple target mRNAs, and the Qrr

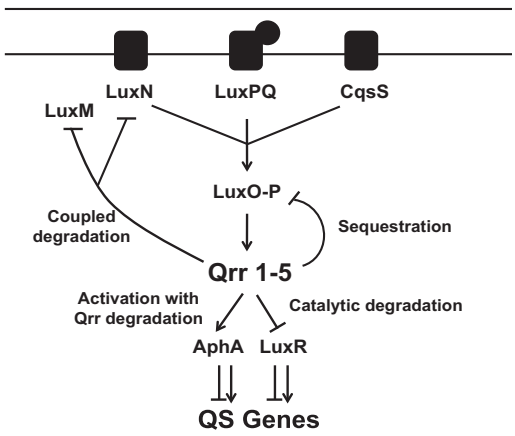

Figure 1. Schematic for How a *V. harveyi* Quorum-Sensing Qrr sRNA Uses Four Regulatory Mechanisms to Control Target mRNAs

At low cell density, the three quorum-sensing receptors LuxN, LuxPQ, and CqsS transfer phosphate through LuxU (not shown) to LuxO. Phosphorylated LuxO activates transcription of genes encoding five sRNAs called Qrr1–Qrr5. Using Qrr3 as the representative quorum-sensing regulatory sRNA, we show that the Qrr sRNA catalytically represses the high-cell-density master regulator *luxR*. The Qrr sRNA represses *luxO* through sequestration. The Qrr sRNA represses the *luxMN* operon through coupled degradation (*luxM* encodes the synthase that produces the ligand for LuxN). The Qrr sRNA also activates translation of the low-cell-density master regulator *aphA*; base-pairing with the *aphA* mRNA leads to Qrr degradation.

sRNAs act as both positive and negative regulators. These features enable us to exploit this set of sRNAs and their particular mRNA targets to dissect pairing regimes, target preferences, and modes of regulation. The Qrr sRNAs positively control the production of the low-cell-density master regulator AphA and they repress the production of the high-cell-density master regulator LuxR (Rutherford et al., 2011; Tu and Bassler, 2007). The Qrr sRNAs feed back to repress the genes encoding one of the quorum-sensing synthase-receptor pairs, LuxMN, and the gene encoding the transcription factor LuxO (Teng et al., 2011; Tu et al., 2010). The Qrr sRNAs also posttranscriptionally regulate sixteen genes outside of the quorum-sensing circuit (Shao et al., 2013).

In the present study, we show that a representative Qrr sRNA, Qrr3, uses four distinct mechanisms to regulate four different target mRNAs. The Qrr3 sRNA undergoes coupled degradation when it pairs with *luxM* mRNA, it uses sequestration to control *luxO* mRNA, it catalytically represses *luxR* mRNA, and it activates *aphA* mRNA expression while the Qrr3 sRNA itself is degraded. The mRNA targets that reduce Qrr sRNA stability (*luxM* and *aphA*) do so by remodeling the 5′-most stem-loop of the Qrr sRNA. mRNA targets that sequester the Qrr sRNA *(luxO*) presumably do so via tight binding to the Qrr sRNA. Indeed, we demonstrate that a particular regulatory mechanism can be converted into a different one by altering the base-pairing position or binding strength. The different sRNA-target mRNA interaction mechanisms result in distinct regulatory strength and dynamical behaviors of the mRNA targets in vivo. Furthermore, the particular regulatory mechanism used for mRNA target regulation is critical for properly timed quorum-sensing responses.

RESULTS

The Qrr3 sRNA Uses Distinct Mechanisms to Regulate Different mRNA Targets

There are 20 known targets of the *Vibrio harveyi* Qrr sRNAs (Shao et al., 2013), four of which, *luxM*, *luxO*, *luxR*, and *aphA*, are members of the quorum-sensing regulatory circuit and are the focus of this work (Figure 1). Little is known about how the five Qrr sRNAs choose among their mRNA targets in vivo. To investigate Qrr target preferences, we developed a competition assay in *Escherichia coli*. We constructed a dual reporter system on a single plasmid that encodes (1) an isopropyl β-D-1-thiogalactopyranoside (IPTG)-inducible 5′UTR-GFP fusion to a Qrr-repressed mRNA target (the Qrr "target" in all assays), and (2) an arabinose inducible 5′UTR-mCherry fusion to a different Qrr-controlled mRNA target (the Qrr "competitor"). We transformed this dual reporter plasmid along with a second plasmid encoding anhydrotetracycline-inducible Qrr3 into *E. coli* (Figure S1A available online; Tables S1, S2, and S3). The five Qrr sRNAs are similar in sequence and secondary structure and they share most of the target mRNAs (Shao et al., 2013; Tu and Bassler, 2007). We arbitrarily chose Qrr3 to use in these assays.

To monitor Qrr preference, we first measured GFP fluorescence from the target mRNA in the absence of both Qrr3 and competitor mRNA to determine the basal expression level of the mRNA target. Next, we measured target GFP fluorescence when Qrr3 was induced to determine the level of target mRNA repression by Qrr3. Finally, we measured GFP fluorescence from the target mRNA when Qrr3 was induced and, additionally, the competitor mRNA was induced to different levels. This third measurement allowed us to assess the ability of different competitor mRNAs to compete with the target mRNA for regulation by Qrr3. Our expectation was that, in the case of a Qrr3 repressed target mRNA, if competition occurred, the target mRNA-GFP fluorescence should increase when we induced expression of the competitor mRNA because the amount of Qrr3 available to regulate the target mRNA would decrease. By contrast, if the target mRNA-GFP level did not change when we induced expression of the competitor mRNA, we would infer that the competitor mRNA did not compete with the target mRNA for regulation by Qrr3.

Our dual reporter system allowed us to simultaneously measure mCherry production from the competitor mRNA. A change in mCherry level following induction of Qrr3 was useful to verify that the competitor was indeed being regulated by Qrr3. We also determined the expression level and the half-life of Qrr3 in the absence and presence of the mRNA targets. Likewise, we measured the expression level of the target mRNAs in the absence and presence of Qrr3. These final measurements allowed us to discover the fates of Qrr3 and the target mRNA, and thus the mechanism used by Qrr3 to control each target—catalytic, coupled degradation, sequestration, or mRNA activation with concomitant sRNA degradation.

Using this strategy, we first investigated whether *luxM* mRNA competes with *luxR* mRNA for regulation by Qrr3. As a control, we show that, in the absence of Qrr3, increasing the *luxM-mCherry* production does not significantly alter LuxR-GFP production (Figure 2A, open circles). When Qrr3 is present, LuxR-GFP is

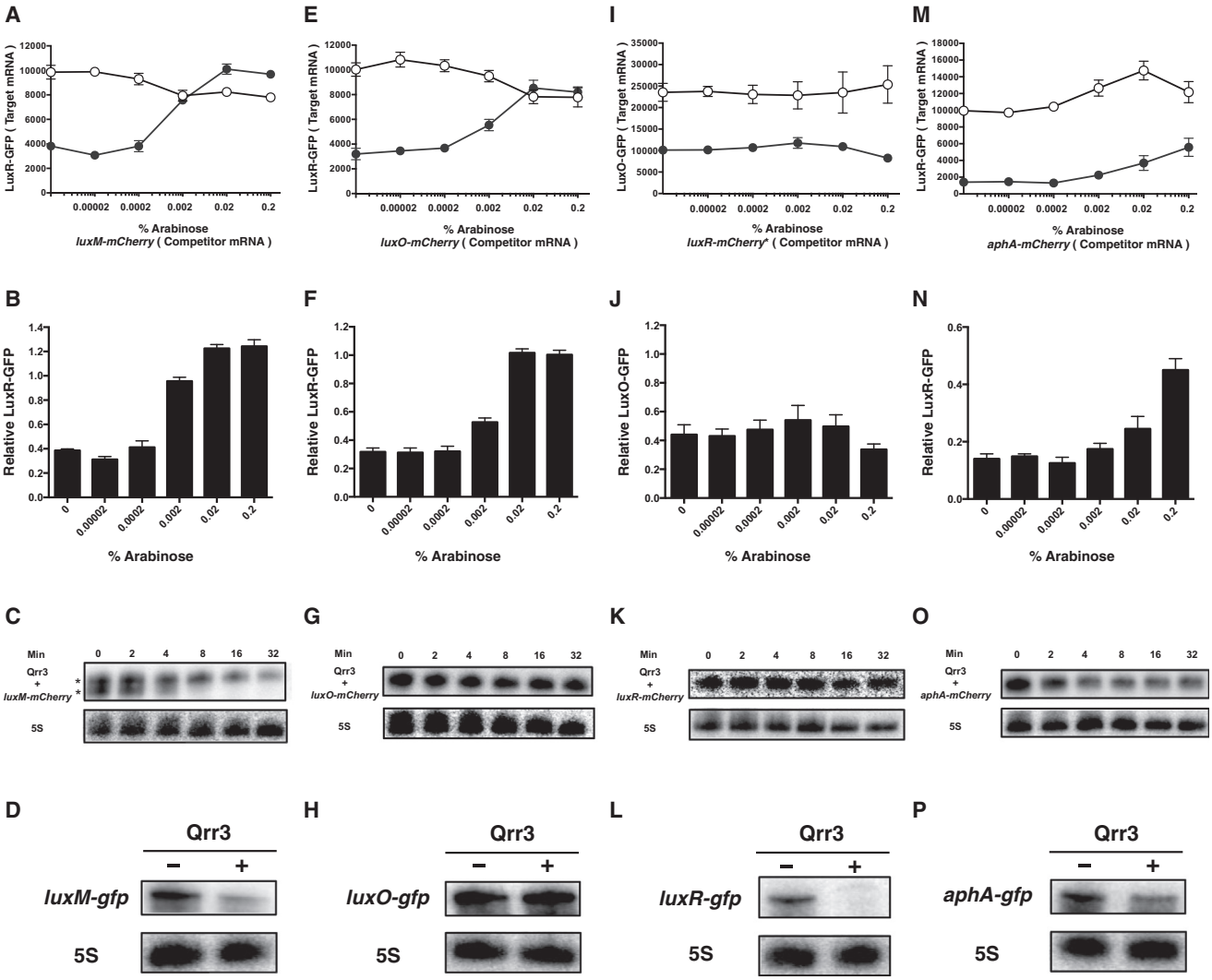

Figure 2. mRNAs Have Different Abilities to Compete for Qrr sRNA Regulation

(A, E, I, and M) Competition between different Qrr sRNA target mRNAs. Fluorescence from a plasmid-borne *luxR-gfp* (A, E, and M) or *luxO-gfp* (I) translational fusion was measured in *E. coli*. Experiments were performed in the absence of Qrr3 (open circles) and in the presence of Qrr3 (filled circles). Arabinose was added to drive production of the competitor mRNA *luxM-mCherry* (A), *luxO-mCherry* (E), *luxR-mCherry** (I), and *aphA-mCherry* (M). Means and SEM for triplicate cultures are shown.

(B, F, J, and N) Quantification of the fractional expression of LuxR-GFP (B, F, and N) or LuxO-GFP (J) from (A), (E), (M), and (I), respectively. GFP fluorescence in the presence of Qrr3 was normalized to that in its absence. Means and SEM for triplicate cultures are shown.

(C, G, K, and O) Half-life of Qrr3 in the presence of *luxM-mCherry* (C), *luxO-mCherry* (G), *luxR-mCherry* (K), and *aphA-mCherry* (O).

(D, H, L, and P) Northern blots of *luxM-gfp* (D), *luxO-gfp* (H), *luxR-gfp* (L), and *aphA-gfp* (P) translational fusions in the absence (−) and presence (+) of Qrr3. For all Northern blots, results are representative of two independent experiments and 5S rRNA was used as the loading control.

See also Figures S1, S2, and S3.

repressed 2.5-fold in the absence of *luxM-mCherry* (Figures 2A, filled circles, and 2B; no arabinose). Inducing *luxM-mCherry* expression causes an increase in LuxR-GFP (Figures 2A, filled circles, and 2B). This result shows that *luxM* mRNA successfully competes with *luxR* mRNA for regulation by Qrr3. We confirmed that in the absence of Qrr3, increasing the arabinose inducer results in increasing production of *luxM-mCherry* (Figure S1B, open circles). At low arabinose concentration and thus low *luxM-mCherry* levels, LuxM-mCherry is repressed 2.5-fold in the presence of Qrr3 (Figure S1C). By contrast, at high arabinose, and thus high *luxM-mCherry* levels, neither LuxM-mCherry nor LuxR-GFP is repressed by Qrr3 (Figures 2B and S1C). Presumably, under the latter condition, Qrr3 is saturated by the competitor mRNA or degraded. In analogous experiments, we measured the ability of *luxM-mCherry* to compete with *luxO-gfp* and with *luxM-gfp* for regulation by Qrr3 and obtained similar results (Figures S2A and S2B). Thus, *luxM* mRNA can successfully compete for regulation by Qrr3 against *luxM* (itself), *luxO*, and *luxR* mRNA.

To assess what becomes of Qrr3 when regulating the *luxM-mCherry* target mRNA, we measured Qrr3 levels in the absence

and presence of *luxM-mCherry* mRNA. When no *luxM-mCherry* mRNA is present, Qrr3 appears as one band on a Northern blot (Figure S3A, left lane). In the presence of *luxM-mCherry* mRNA, two Qrr3 bands appear, suggesting that Qrr3 is processed (Figure S3A, right lane). In the absence of any mRNA target, the Qrr3 half-life is over 32 min (Figure S3B). In the presence of *luxM-mCherry* mRNA, the half-lives of both Qrr3 RNA bands decrease, with the processed Qrr3 product exhibiting the most dramatic decline (to $t_{1/2}$ <8 min, Figure 2C). Together, these data explain how *luxM* mRNA competes with *luxR* mRNA for regulation by Qrr3: the presence of *luxM* mRNA causes Qrr3 degradation, decreasing the amount of Qrr3 available to regulate *luxR* mRNA. We also examined what becomes of the *luxM* mRNA during regulation by Qrr3. We used *gfp* fusions to measure target mRNA levels. Both the *luxM-gfp* mRNA (Figure 2D) and the LuxM-GFP protein (Figure S1D) decreased in the presence of Qrr3, indicating that *luxM* mRNA is degraded during regulation. We therefore conclude that Qrr3 regulates *luxM* mRNA through a coupled degradation mechanism: when base-paired, both the *luxM* mRNA target and the Qrr3 sRNA are subject to degradation.

We next investigated whether *luxO* mRNA can compete with other mRNA targets for Qrr3 regulation. We again used *luxR-gfp* mRNA as the "target" for which we show data, but we note that the results are the same when *luxM-gfp* or *luxO-gfp* mRNAs act as the "target" (data not shown). Figures 2E, 2F, S1E, and S1F show that *luxO* mRNA can indeed compete with *luxR* mRNA for Qrr3 regulation, similar to what we found above when *luxM-mCherry* acts as the competitor. However, unlike when *luxM-mCherry* was the competitor, the level and half-life of Qrr3 are identical in the absence and presence of *luxO-mCherry* competitor mRNA (Figures 2G, S3B, and S3C) and no processed Qrr3 RNA band was detected (Figures 2G and S3C). Furthermore, the presence of Qrr3 does not alter *luxO-gfp* mRNA levels (Figure 2H), however, LuxO-GFP protein production is repressed ~15-fold in the presence of Qrr3 (Figure S1G). Based on these data, we propose that Qrr3 and *luxO* mRNA sequester one another when base-paired.

We likewise tested whether *luxR* mRNA could act as a competitor. Induction of high *luxR-mCherry* caused significant reductions in target-GFP levels even in the absence of Qrr3 suggesting that high levels of the LuxR-mCherry protein are toxic. To circumvent this problem, we introduced a stop codon in *mCherry* to abolish mCherry protein production. We call this construct *luxR-mCherry**. When the *luxR-mCherry** mRNA is the competitor, it does not affect Qrr regulation of *luxO-gfp* (Figures 2I and 2J) or *luxR-gfp* (Figures S2C and S2D). Importantly, Figures S1H and S1I show that the *luxR-mCherry** construct is induced by arabinose and is fully repressed by Qrr3. Thus, even though *luxR-mCherry** is capable of interacting with Qrr3, it cannot compete with *luxO-gfp* mRNA or *luxR-gfp* mRNA for Qrr-regulation. To eliminate the possibility that this lack of competition is due to the *mCherry** mutation, we inserted the same stop codon into the *luxM-mCherry* construct. We call this *luxM-mCherry**. *luxM-mCherry** mRNA remains fully capable of competing for Qrr regulation against *luxO-gfp* mRNA (Figures S2E and S2F) and *luxR-gfp* mRNA (Figures S2G and S2H). As controls, we show that the *luxR-mCherry** mRNA is expressed at levels comparable to the *luxM-mCherry*, *luxO-mCherry* and *luxM-mCherry** mRNAs (Figure S2I). Thus, we conclude that *luxR* mRNA does not compete with other mRNA targets for Qrr regulation. Figures 2K and S3D show that *luxR* mRNA does not affect Qrr stability because both the Qrr3 level and its half-life are identical in the absence and presence of *luxR-mCherry* mRNA (or *luxR-mCherry** mRNA; data not shown). By contrast, the level of *luxR-gfp* mRNA decreased in the presence of Qrr3 (Figure 2L), and Qrr3 repressed LuxR-GFP protein production (Figure S1J). These data indicate that Qrr3 causes degradation of *luxR* mRNA. However, the Qrr itself is not degraded and is thus available to regulate other targets. Therefore, we propose that Qrr3 acts catalytically on *luxR* mRNA.

Finally, the Qrr sRNAs posttranscriptionally activate AphA production by base-pairing to *aphA* mRNA (Rutherford et al., 2011; Shao and Bassler, 2012). To test if an activated target can compete for Qrr regulation, we performed our competition assay using *luxR-gfp* as the target mRNA and *aphA-mCherry* as the competitor mRNA. The endogenous expression level of *aphA-mCherry* mRNA is much lower than other competitor mRNA targets (data not shown). We therefore introduced an additional plasmid carrying the identical arabinose inducible *aphA-mCherry* construct into *E. coli* to boost *aphA-mCherry* mRNA levels. Figures 2M and 2N show that *aphA* can compete for regulation by Qrr3. Specifically, Qrr repression of LuxR-GFP decreased from 7-fold to 2-fold (Figure 2N). AphA-mCherry was activated by Qrr3, indicating that *aphA* is regulated by Qrr3 during the competition (Figures S1K and S1L). Qrr3 levels declined and the Qrr3 stability dramatically decreased when *aphA-mCherry* mRNA was present (Figures 2O, S3E, and S3F). Notably, Qrr3 levels reached a plateau after 4 min. We suspect that during the first 4 min there exists *aphA-mCherry*, which fosters Qrr3 degradation. However, after 4 min, there is likely little or no *aphA-mCherry* mRNA remaining to promote Qrr3 degradation. Thus, the Qrr3 level remains stable from that point onward. We also measured what becomes of the *aphA-gfp* mRNA in the absence and presence of Qrr3. Although AphA-GFP protein production is activated ~2.5-fold by Qrr3 (Figure S1M), the full-length *aphA-gfp* mRNA decreased ~2.5-fold in the presence of Qrr3 (Figure 2P). We suggest that when Qrr3 pairs with the *aphA* mRNA, *aphA* translation is activated while Qrr3 is destabilized. The fate of the *aphA* mRNA is unclear and is under investigation.

Together, the above experiments demonstrate that Qrr3 uses four different mechanisms to regulate its mRNA targets: Qrr3 represses *luxM* mRNA through coupled degradation, *luxR* mRNA through catalytic degradation, *luxO* mRNA through sequestration, and Qrr3 activates *aphA* mRNA translation while the Qrr is itself degraded (Figure 1).

mRNA Pairing to Particular sRNA Stem-Loops Dictates the Qrr sRNA Half-Life

We considered what features of the Qrr-mRNA pairs dictate the Qrr fate. *luxM* base pairs with the first and second stem-loops (SL1+SL2) of the Qrr, *aphA* base pairs with SL1, and *luxR* and *luxO* base pair with SL2 (Figures 3A1–3A5) (Rutherford et al., 2011; Shao and Bassler, 2012; Teng et al., 2011; Tu and Bassler, 2007; Tu et al., 2010). 5′ stem-loops commonly protect mRNAs from RppH- and RNase E-mediated degradation (Belasco, 2010). We have previously shown that this same

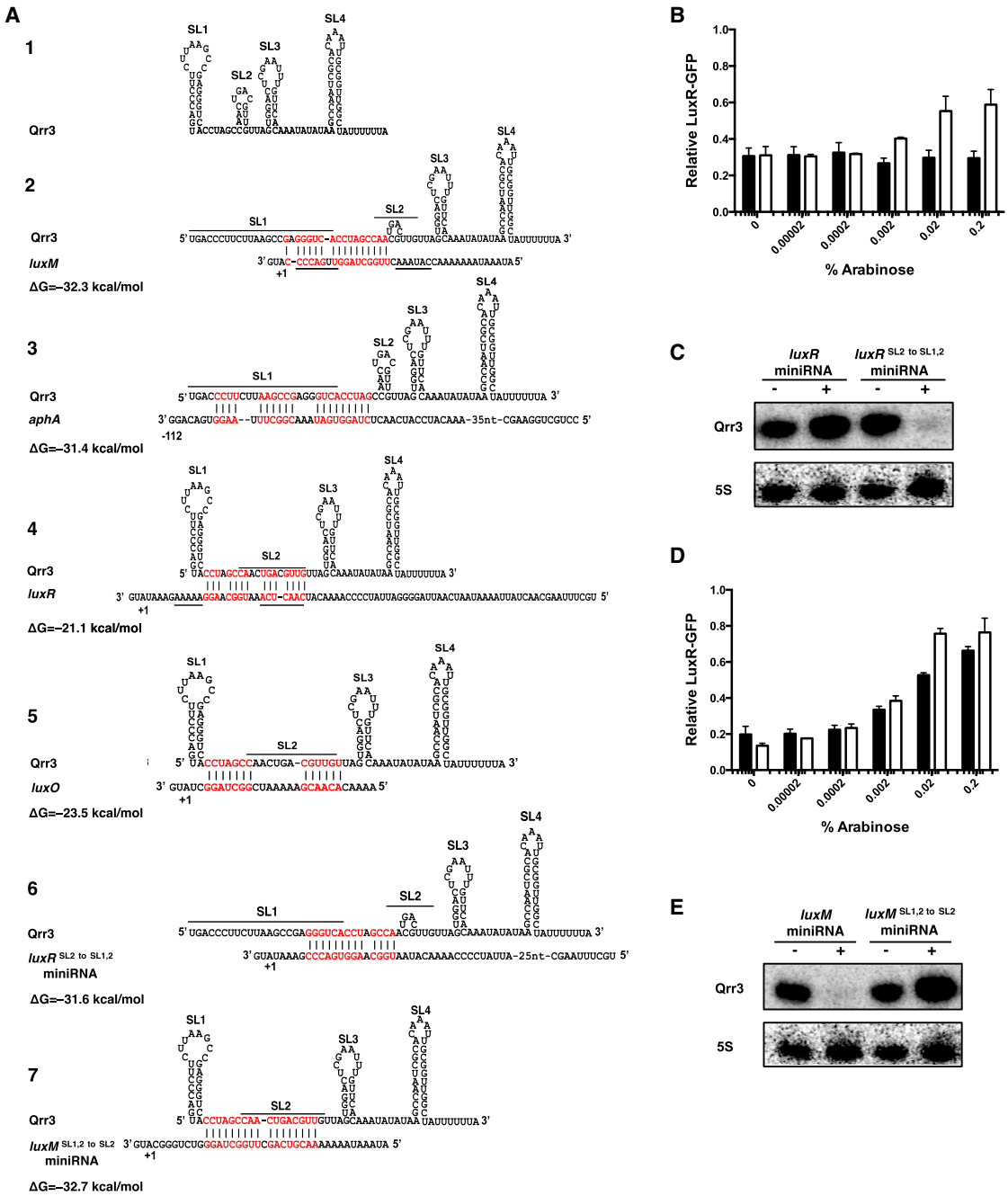

Figure 3. Base-Pairing to the 5′ Stem-Loop of Qrr3 Leads to Qrr Degradation

(A) Predicted secondary structure of Qrr3 and base-pairing patterns with the target mRNAs. The four predicted stem-loops of Qrr3 are labeled SL1, SL2, SL3, and SL4. Melted loops are shown with overlines. Base-pairing patterns and energies for Qrr3 and target mRNAs were predicted by RNAhybrid (http://bibiserv.techfak.uni-bielefeld.de/rnahybrid/). Nucleotides involved in base-pairing are labeled red. Nucleotides mutated to make the miniRNAs (see Extended Experimental Procedures) are shown with underlines. Translational start sites are denoted +1.

(B) Competition for Qrr3 regulation between the *luxR* miniRNA (black bars) or the *luxR* $^{SL2\ to\ SL1,2}$ miniRNA (white bars) and *luxR-gfp*.

(C) Northern blot showing Qrr3 levels in the absence (–) and presence (+) of the *luxR* miniRNA or the *luxR* $^{SL2\ to\ SL1,2}$ miniRNA.

(D) Competition between the *luxM* miniRNA (black bars) or the *luxM* $^{SL1,2\ to\ SL2}$ miniRNA (white bars) for Qrr3 regulation of *luxR-gfp*.

(E) Northern blot showing Qrr3 levels in the absence (–) and presence (+) of the *luxM* miniRNA or the *luxM* $^{SL1,2\ to\ SL2}$ miniRNA. For (B) and (D), means and SEM for triplicate cultures are shown. Normalization as in Figure 2. For (C) and (E), results are representative of two independent experiments.

See also Figures S3 and S4.

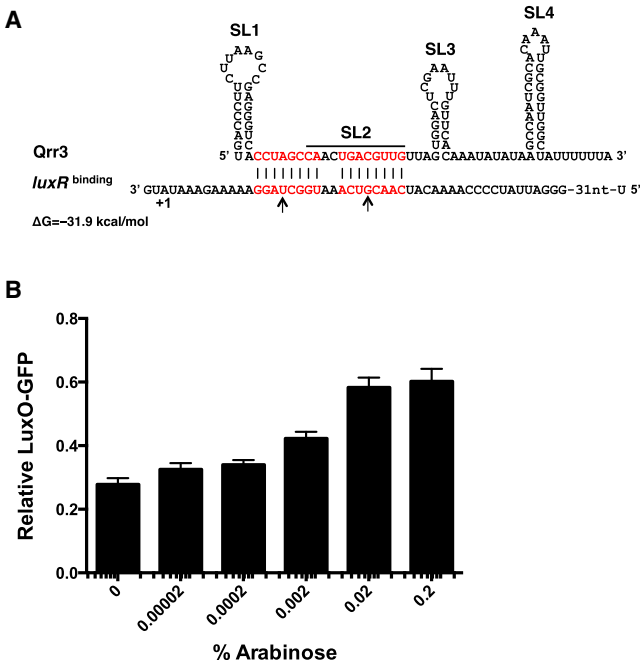

Figure 4. The Binding Strength of the Qrr sRNA-Target mRNA Pair Determines Sequestration versus Catalytic Degradation

(A) Base-pairing between Qrr3 and *luxR*^{binding} mRNA. Designations as in Figure 3A. Mutated nucleotides are labeled with arrows.

(B) Competition between *luxR*^{binding}*-mCherry** and *luxO-gfp* for Qrr3 regulation. *luxR*^{binding}*-mCherry** was driven by the arabinose promoter. Means and SEM for triplicate cultures are shown. Normalization as in Figure 2.

mechanism is also used to protect the Qrr sRNAs from degradation. Deletion of SL1 or mutations that disrupt SL1 base-pairing destabilize the Qrr sRNAs, and mutations that restore SL1 base-pairing restore Qrr stability in *E. coli* (Shao et al., 2013) and in vivo in *V. harveyi* (Figure S3G). We wondered whether base-pairing to the target mRNA, if it leads to melting of SL1, causes Qrr degradation. To test this possibility, we constructed miniRNAs containing only the 5′UTRs of selected mRNA targets linked to transcription terminators. We used miniRNAs to eliminate ribosome-mediated mRNA stabilization effects. Using the above competition assay, we found that the *luxR* miniRNA does not affect Qrr3 repression of *luxR-gfp*, which is consistent with a catalytic regulatory mechanism (Figure 3B, black bars). However, shifting the Qrr3-*luxR* base-pairing from SL2 to SL1+SL2 (Figure 3A6) confers competition capability to the *luxR* $^{SL2\ to\ SL1,2}$ miniRNA (Figure 3B, white bars). The presence of the *luxR* miniRNA did not affect the level of Qrr3, however, the presence of the *luxR* $^{SL2\ to\ SL1,2}$ miniRNA caused a decrease in Qrr3 level (Figure 3C).

We also constructed a *luxM* miniRNA and found that it competes with *luxR-gfp* for Qrr regulation identically to the full-length *luxM-mCherry* mRNA fusion (Figure 3D, black bars). Qrr3 was degraded in the presence of the *luxM* miniRNA as shown by its decreased expression level (Figure 3E). A construct that retains the number of base-pairing nucleotides but moves the base-pairing region from SL1+SL2 to SL2 eliminated the ability of the *luxM* $^{SL1,2\ to\ SL2}$ miniRNA to induce Qrr degradation (Figures 3A7 and 3E). Together, these data suggest that pairing to, and presumably remodeling of SL1 causes Qrr degradation, while pairing to SL2 does not. As controls, we show that the *luxR*, *luxR* $^{SL2\ to\ SL1,2}$, *luxM*, and *luxM* $^{SL1,2\ to\ SL2}$ miniRNAs are expressed (Figures S4A and S4C, respectively), regulated by Qrr3 (Figures S4B and S4D, respectively), and the *luxR* $^{SL2\ to\ SL1,2}$ and *luxM* $^{SL1,2\ to\ SL2}$ miniRNAs behave identically to the *luxR* $^{SL2\ to\ SL1,2}$ and *luxM* $^{SL1,2\ to\ SL2}$ mRNAs, respectively (Figure S4E).

To map the processing site in the Qrr sRNA when base-paired to *luxM*, we expressed steady-state levels of Qrr3, induced target mRNA expression, and monitored the dynamics of Qrr decay. Consistent with *luxM* mRNA being controlled by coupled degradation and *luxR* mRNA being controlled by a catalytic mechanism, a Qrr sRNA degradation product appeared within ten minutes of induction of *luxM* mRNA (Figure S3H) whereas Qrr3 was not degraded following *luxR* mRNA induction (Figure S3H). Primer extension analysis revealed that processing occurred in the Qrr SL1 region after nucleotides C (position 5), U (position 7), and U (position 8) (Figure S3I, red arrows), suggesting that opening the SL1 structure makes the RNase cleavage sites accessible.

We did not observe processing of the Qrr sRNA when *aphA* was expressed (Figures 2O, S3E, and S3F) presumably because the cleavage sites are involved in base-pairing to the *aphA* mRNA (Figure 3A3). This arrangement likely shields the sites from cleavage. We wondered whether partial opening of SL1 in a way that does not reveal the cleavage sites is sufficient to induce Qrr degradation. We constructed mutations (GAC to CUG at positions 2 to 4) to partially open SL1 (Figure S3J) and mimic when *aphA* is base-paired. We call this construct Qrr3mut. The Qrr3mut sRNA is unstable (Figure S3J) compared to wild-type Qrr3 (Figure S2B) and degraded without an apparent cleavage product.

The Qrr-mRNA Base-Pairing Strength Determines Whether an mRNA Target Will Sequester the Qrr sRNA

The *luxM* $^{SL1,2\ to\ SL2}$ miniRNA does not induce Qrr degradation (Figure 3E). Yet, unlike the *luxR* miniRNA, the *luxM* $^{SL1,2\ to\ SL2}$ miniRNA is capable of competing with *luxR-gfp* mRNA for Qrr regulation (Figure 3D, white bars). These data suggest that the *luxM* $^{SL1,2\ to\ SL2}$ miniRNA competes for Qrr regulation by sequestering the Qrr sRNA. Comparison of the predicted binding energies of *luxM* $^{SL1,2\ to\ SL2}$ miniRNA, *luxR* mRNA, and *luxR* miniRNA (the base pairing region in the *luxR* mRNA and the *luxR* miniRNA is identical) to Qrr3 reveals that the Qrr3-*luxM* $^{SL1,2\ to\ SL2}$ miniRNA duplex (−32.7 kcal/mol) is more stable than the Qrr3-*luxR* mRNA (or *luxR* miniRNA) duplex (−21.1 kcal/mol) (Figures 3A7 and 3A4). We wondered whether mRNA targets that bind strongly to SL2 of Qrr3 sequester the Qrr sRNA, whereas targets with lower binding energy are catalytically degraded. If so, this could explain why some targets can compete for Qrr regulation while others cannot. To test this hypothesis, we introduced two point mutations into the *luxR-mCherry** mRNA 5′UTR to increase its strength of binding to Qrr3 (−31.9 kcal/mol) (Figure 4A). We call this construct *luxR*^{binding}*-mCherry**. Indeed, *luxR*^{binding}*-mCherry** gains the capability to compete with *luxO-gfp* mRNA for Qrr regulation (Figure 4B, compare to Figure 2J). As a control, we show that the *luxR*^{binding}*-mCherry** mRNA is made at levels comparable to that of *luxR-mCherry** mRNA (Figure S2I). We suggest that the base-pairing strength between an mRNA target

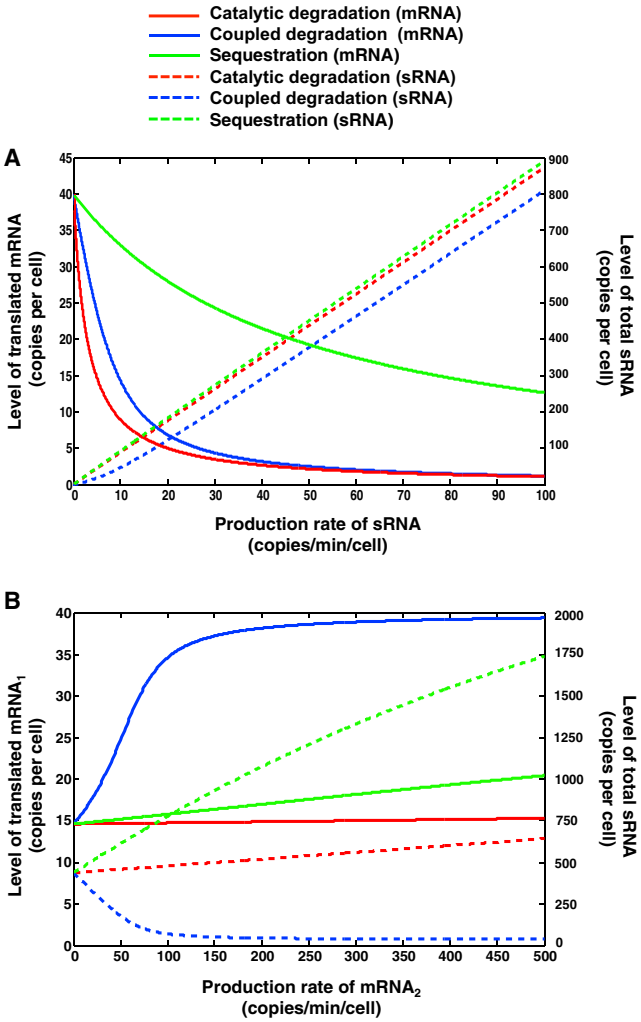

Figure 5. Modeling the Strength and Competition Capacity of the Different sRNA Regulatory Mechanisms

(A) The levels of translated mRNA (solid curves) and total sRNA (dashed curves) plotted against the production rate of the sRNA, based on Equations S1, S2, S3, S4, S5, and S6.

(B) The levels of translated $mRNA_1$ (solid curves) and total sRNA (dashed curves) are plotted against the production rate of the competitor $mRNA_2$ based on Equations S1, S2, S3, S4, S5, and S6. In (A) and (B), three different regulatory mechanisms are explored: catalytic degradation (red), coupled degradation (blue), and sequestration (green).

and the Qrr sRNA governs whether an mRNA target will sequester the Qrr sRNA and thus compete for its regulation against other target mRNAs.

The Different Qrr Regulatory Mechanisms Govern Competition and Potency of Target Control

We used mathematical modeling to explore the consequences of the distinct sRNA-mRNA interaction modes on the different RNA species and the underlying biological process being regulated. This initial modeling effort is focused on sRNA-mediated repression because sRNA-directed activation is not yet well characterized. Based on experimental evidence from previous studies, we assume that Hfq protein complexes are always close to saturated by sRNAs and mRNAs (Hussein and Lim, 2011; Moon and Gottesman, 2011), but that individual sRNA and mRNA molecules actively cycle on and off of Hfq complexes (Fender et al., 2010; Wagner, 2013).

We first modeled the scenario of a single species of sRNA (e.g., a single Qrr) specifically regulating a single type of mRNA target, in the presence of a background of noncognate sRNAs and mRNAs (see Supplemental Information and Table S4). In Figure 5A, we show as solid curves the copy number of mRNA molecules available for translation, which are the free mRNA molecules and the mRNA molecules bound to Hfq with noncognate sRNAs, versus the production rate of the sRNA. We find that an mRNA target regulated by catalytic degradation (red) is the most efficiently repressed by the sRNA, followed by an mRNA regulated by coupled degradation (blue). An mRNA controlled by sequestration (green) exhibits only moderate repression by the sRNA. Moreover, mRNA targets that are regulated by coupled degradation decrease the total sRNA level (dashed blue curve). Specifically, the total sRNA level remains suppressed by coupled degradation until sRNA production exceeds the expected threshold of ~7.5 copies/min/cell and then increases linearly. (The threshold occurs where the sRNA production rate/the sRNA degradation rate in the sRNA-Hfq-mRNA complex equals the mRNA production rate/the mRNA degradation rate in the sRNA-Hfq-mRNA complex). This threshold-linear behavior of total sRNA does not occur in the cases of regulation by catalytic degradation or sequestration (red and green dashed curves, respectively).

We next modeled the scenario in which competition occurs between different mRNA targets for sRNA regulation (see Supplemental Information). In our system, we have one target mRNA ($mRNA_1$) and one competitor mRNA ($mRNA_2$). Our modeling results show that coupled degradation supplies the most efficient competition: the level of translated $mRNA_1$ increases with the production rate of $mRNA_2$ (Figure 5B, solid blue curve), followed by sequestration (Figure 5B, solid green curve). Catalytic degradation provides only minimal competition (Figure 5B, solid red curve). This result is in good qualitative agreement with our experimental data in which *luxM* and *luxO* mRNAs compete for Qrr regulation and *luxR* mRNA is nearly incapable of competing for Qrr regulation. We also examined the total sRNA level when we increased the production rate of the competitor $mRNA_2$ (Figure 5B, dashed curves). As expected, coupled degradation results in a significant decrease in sRNA level (Figure 5B, dashed blue curve). The increase of the total sRNA level in the case of sequestration is due to the sequestering $mRNA_2$ partially protecting the sRNA from degradation (Figure 5B, dashed green curve).

The Different Qrr Regulatory Mechanisms Govern the Dynamics of Target mRNA Expression

To examine the effect of different regulatory mechanisms on the dynamics of target regulation, we modeled a situation in which sRNA production is induced at time zero and then terminated after 2 hr. We found that when sRNA production is induced (Figure 6A, dashed curves), catalytic degradation and coupled degradation provide the most rapid mRNA and protein

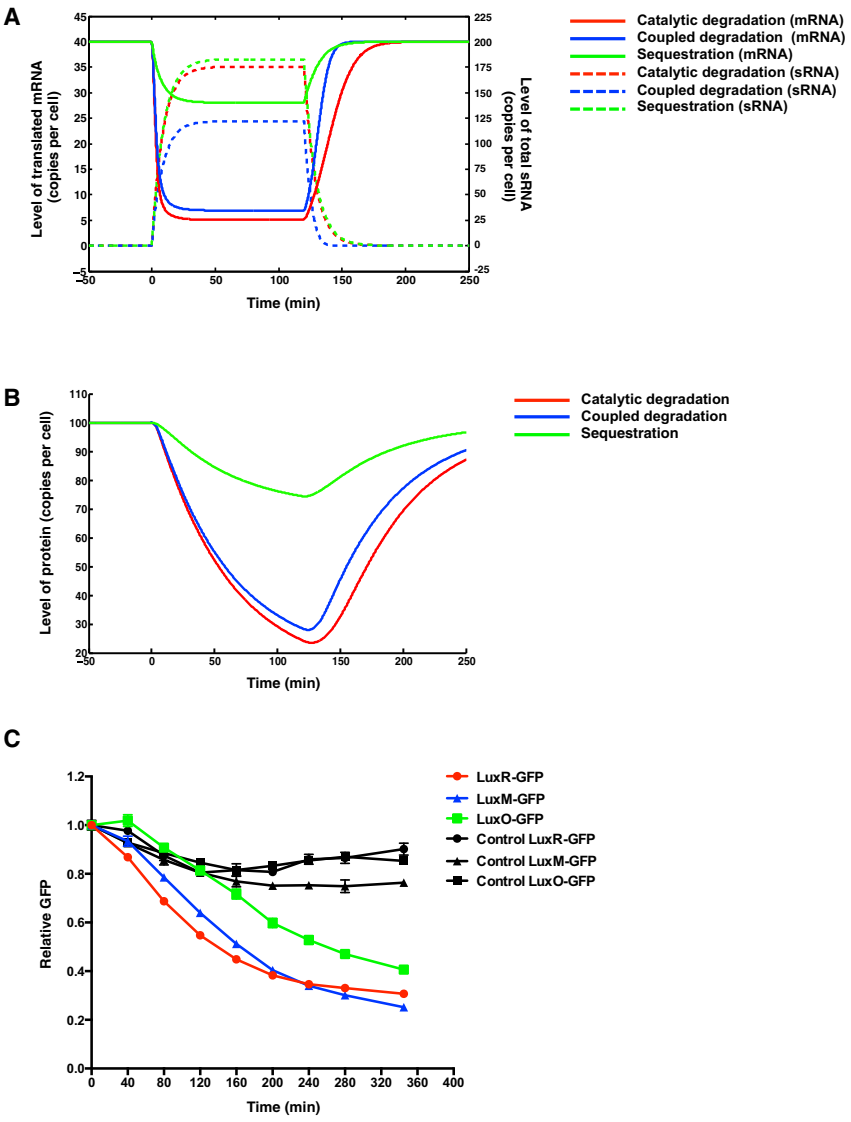

Figure 6. mRNA Target Dynamics Provided by the Different sRNA Regulatory Mechanisms

(A) The levels of translated mRNA (solid curves) and total sRNA (dashed curves) are plotted over time based on Equations S1, S2, S3, S4, S5, and S6.

(B) The level of regulated protein is plotted over time based on Equations S1, S2, S3, S4, S5, S6, and S9. sRNA production is induced at time zero and is terminated at 120 min. Three different regulatory mechanisms are explored: catalytic degradation (red), coupled degradation (blue), and sequestration (green).

(C) Repression of target mRNAs following Qrr sRNA induction. GFP fluorescence at each time-point was normalized to mCherry fluorescence, and the relative normalized GFP levels are plotted. The results are LuxR-GFP: red and black (control) circles, LuxM-GFP: blue and black (control) triangles, LuxO-GFP: green and black (control) squares. Means and SEM from three independent cultures are shown. See also Figure S5.

response, while sequestration confers the slowest response (Figures 6A, solid curves, and 6B; Supplemental Information). By contrast, when sRNA production is terminated, catalytic degradation yields the slowest recovery. As expected, sequestration affects the translated mRNA level but it does not affect the total mRNA level. Catalytic degradation and coupled degradation affect both mRNA translation and overall target mRNA levels (Figure S5). In all cases, repression of mRNA is rapid (~10 min) (Figure 6A, solid curves), whereas repression of protein is slow—approaching steady state only after hours—due to the slow dilution rate of protein (Figure 6B). These predictions are in agreement with existing experimental data (Papenfort et al., 2013; Vanderpool and Gottesman, 2004).

With respect to the mRNA targets studied here, the model predicts that *luxR* mRNA will be the most sensitive to changes in Qrr levels because it is controlled by catalytic degradation. Thus, during the high-cell-density to low-cell-density transition, when the Qrr sRNAs are produced, *luxR* mRNA should respond more rapidly to changes in Qrr levels than do *luxM* and *luxO* mRNAs. To test the predictions of the model, we constructed three *V. harveyi* strains that report on target mRNA levels by integrating a *luxR*, a *luxM*, or a *luxO* 5′UTR translational GFP fusion under a constitutive promoter onto the chromosome. We used *mCherry* oriented in the opposite direction to normalize for cellular protein (Long et al., 2009). We measured GFP and mCherry fluorescence after we induced Qrr production by adding a quorum-sensing antagonist (see Experimental Procedures) (Shao et al., 2013). Figure 6C shows that the LuxR-GFP protein is indeed the most rapid to respond to Qrr changes, followed by the LuxM-GFP protein, and finally the LuxO-GFP protein. As a control, we measured LuxR-GFP, LuxM-GFP, and LuxO-GFP levels in *V. harveyi* strain lacking all five Qrr sRNAs; GFP did not significantly change following addition of the antagonist.

The Different Qrr Regulatory Mechanisms Are Critical for Quorum-Sensing Circuit Dynamics

Our data and model show that the particular Qrr sRNA mechanism used to regulate each mRNA target dictates the level and dynamics of the target's expression. We expect that these dynamics specify the quorum-sensing response timing in vivo. To investigate this notion, we measured the in vivo dynamical changes of individual quorum-sensing components that occurred in response to alterations in Qrr levels. We measured the mRNA levels and the rates of protein synthesis (see Extended Experimental Procedures and Table S5) of LuxR, LuxO, LuxM, and AphA over a 90 min time period following termination of Qrr production. As controls, we show that the levels of

Qrr1-4 decreased following autoinducer addition (Figure S6A). Qrr5 is not produced under our experimental conditions, so we did not measure it (Tu and Bassler, 2007). Figure 7A shows that, following the addition of the autoinducer, *luxR* mRNA increased ~14-fold and the rate of LuxR protein synthesis increased ~25-fold; *luxO* mRNA does not change within 90 min, however, the rate of LuxO protein production increased 2-fold; *luxM* mRNA increased ~3-fold (we were unable to detect the LuxM protein, likely because the *luxM* gene is partially deleted in this locked strain); *aphA* mRNA decreased ~20-fold and AphA protein synthesis decreased ~4- to 6-fold. These results confirm our prediction that catalytically regulated targets (e.g., *luxR)* undergo larger dynamic range changes than do targets regulated by coupled degradation (e.g., *luxM*). Sequestered targets such as *luxO* are the most weakly regulated.

We next explored how important the specific mechanism is for the quorum-sensing response. We altered the regulatory mechanism by which a particular mRNA target (*luxR*) is controlled and tested the effects on overall quorum-sensing dynamics. To accompany the experiment, we modeled an internal segment of the circuit in which phosphorylated LuxO activates the production of the Qrr sRNAs and the Qrr sRNAs catalytically repress *luxR* mRNA, whereas they sequester *luxO* mRNA (Figure 7B).

The subcircuit equations correspond to those used for one Qrr with two mRNA targets (Supplemental Information), with Qrr production assumed to be proportional to the level of phosphorylated LuxO. The kinetic equation for the Qrr sRNA is therefore:

$$\begin{aligned}\frac{d[Qrr]_{total}}{dt} &= \Gamma_{Qrr}[LuxO \sim P] - \gamma_{Qrr}[Qrr]_{free} \\ &\quad - \gamma_{Qrr:mRNA_0}[Qrr: \ Hfq: \ mRNA_0] \\ &\quad - \gamma_{Qrr:luxO}[Qrr: \ Hfq: \ luxO_m] \\ &\quad - \gamma_{Qrr:luxR}[Qrr: \ Hfq: \ luxR_m].\end{aligned} \qquad \text{(Equation 1)}$$

We added two kinetic equations for LuxO and LuxR protein:

$$\frac{d[LuxO_p]}{dt} = \Gamma_{LuxO_p}[luxO_m] - \gamma_{LuxO_p}[LuxO_p] \qquad \text{(Equation 2)}$$

$$\frac{d[LuxR_p]}{dt} = \Gamma_{LuxR_p}[luxR_m] - \gamma_{LuxR_p}[LuxR_p]. \qquad \text{(Equation 3)}$$

Using these equations, we explored three possible mechanisms for *luxR* regulation: catalytic degradation, coupled degradation, and sequestration. Our choice of parameters is based on the RNA copy numbers we measured (Figure S7) and previous measurement of LuxR protein copy number (Teng et al., 2010) (see Supplemental Information).

In Figure 7C, we plot the prediction for LuxR protein copy number per cell versus the phosphorylated fraction of LuxO ([LuxO ~ P]/[LuxO]). The ratio [LuxO ~ P]/[LuxO] is low in the high-cell-density state and high in the low-cell-density state. Within the model, the catalytic mechanism yields the most efficient repression of LuxR protein, followed by coupled degradation, while sequestration does not achieve the experimentally observed level of LuxR repression. Can sequestration adequately repress LuxR if we allow increased Qrr production? We found that in order to achieve ~10-fold repression of LuxR, the Qrr production rate must be increased ~100-fold (Figure 7C, black curve). Under this condition, LuxO protein is repressed at low cell density to the unrealistically low level of fewer than five copies per cell (Figure 7D, black curve). In effect, converting regulation of LuxR from catalytic degradation to sequestration would require rewiring of much of the quorum-sensing network to achieve the same dynamics. Thus, the modeling results suggest that the particular Qrr sRNA mechanisms used to regulate specific quorum-sensing mRNA targets can be crucial for the integrated operation of the quorum-sensing circuit.

To experimentally validate the prediction from the model, we replaced the 5′UTR of *luxR* with that of *luxM* or *luxO* on the chromosome of a *V. harveyi* strain containing only Qrr3. We note that the levels of LuxR protein produced from the three endogenous 5′UTRs are different. Different levels of LuxR feedback on quorum-sensing circuit components would complicate our analysis (Chatterjee et al., 1996; Tu et al., 2008), thus we isolated LuxR production from feedback by introducing a mutation in LuxR (LuxR R17C) that eliminates DNA binding (van Kessel et al., 2013). Figure 7E shows that *luxR* mRNA regulated by a catalytic (red curve) or coupled degradation (blue curve) mechanism increases from low cell density to high cell density, although coupled degradation provides a smaller dynamic range (~3.5-fold) for *luxR* mRNA than catalytic degradation (~10-fold). *luxR* mRNA regulated by sequestration (green curve) shows no increase during growth, which agrees with our prediction. Over the course of the experiment, Qrr3 levels decrease from low cell density to high cell density and the levels of Qrr3 in the three strains are comparable (Figure S6B). These results show that the regulatory mechanism used for a particular target mRNA (*luxR* in this case) determines the precise timing and amplitude of the quorum-sensing response.

DISCUSSION

sRNAs are ubiquitous regulators in bacterial genetic circuits, primarily functioning to control growth rate and stress responses (Gottesman, 2004). Several well-characterized bacterial sRNAs, such as Spot42, RyhB, RybB, and the Qrr sRNAs each control multiple target mRNAs (Beisel and Storz, 2011; Massé and Gottesman, 2002; Papenfort et al., 2010; Shao et al., 2013; Storz et al., 2011). Here, we use the Qrr3 sRNA to show that a single sRNA can regulate its different targets by distinct mechanisms. The particular mechanism used is defined by the base-pairing strategy the Qrr sRNA employs for the particular mRNA target. Specifically, mRNA targets that base pair with the first stem-loop of the Qrr sRNA cause Qrr degradation, and these targets include both repressed (*luxM*) and activated (*aphA*) targets. mRNA targets that base pair with the second stem-loop of the Qrr sRNA do not cause Qrr degradation. Rather, they sequester the Qrr sRNA if the binding is strong (*luxO*), and they are catalytically regulated if binding is weak (*luxR*). Our combined mathematical modeling and experiments show that the regulatory mechanism used determines the potency of regulation, competition capability, and the temporal dynamics of each target mRNA. These distinct mechanisms are crucial to drive the overall quorum-sensing circuit dynamics.

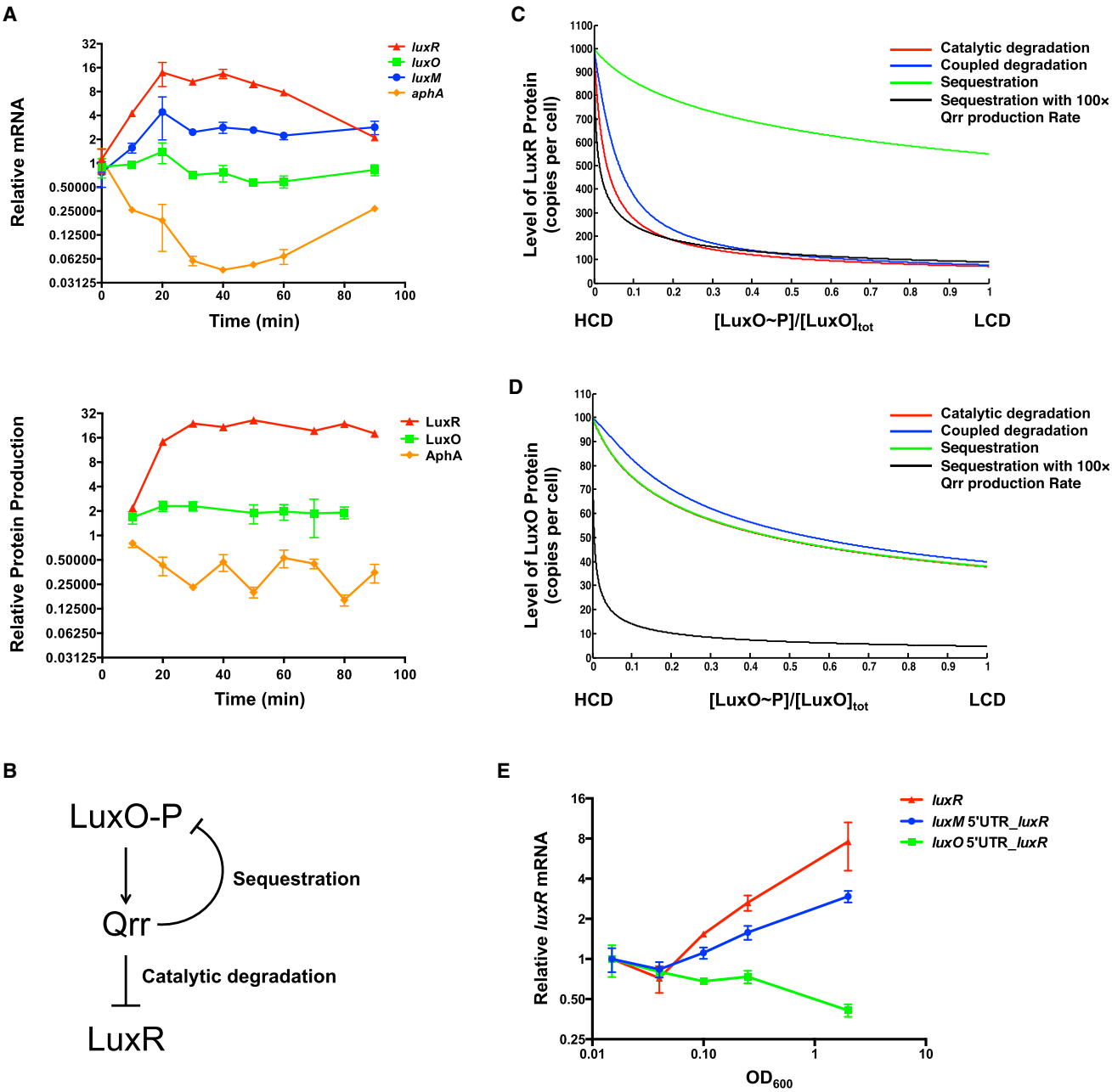

Figure 7. Particular Qrr Regulatory Mechanisms Are Crucial for Proper Quorum-Sensing Dynamics

(A) qRT-PCR and BONCAT of *luxR*, *luxO*, *luxM*, and *aphA* following addition of AI-1 to TL25. Data were normalized to the first time-point in the RNA measurement. Means and SEM from three independent cultures are shown. Relative protein synthesis rates were measured by BONCAT (Supplemental Information) and the evidence for each quantification is provided in Table S5.

(B) Simplified quorum-sensing circuit used for mathematical modeling.

(C and D) LuxR (C) and LuxO (D) protein copy number plotted against the ratio of phosphorylated LuxO to total LuxO protein, based on Equations 1, 2, 3, S1, S2, S3, S4, S5, and S6. In (C) and (D), *luxR* mRNA is regulated by catalytic degradation (red), coupled degradation (blue), or sequestration (green). The black curve shows the case when *luxR* mRNA is regulated by sequestration but the Qrr production rate is increased 100-fold.

(E) qRT-PCR of *luxR* mRNA from *luxR* R17C (red), *luxM* 5′UTR_*luxR* R17C (blue), and *luxO* 5′UTR_*luxR* R17C (green) over growth. Data from each strain were normalized to the first time-point (OD_{600} = 0.015) and plotted against OD_{600}. Means and SEM from four independent cultures are shown.

See also Figures S6 and S7 and Table S5.

In terms of deployment of this set of regulatory mechanisms, we suspect that mRNA targets that require complete and immediate repression will likely be regulated either catalytically or by coupled degradation. Growth and stress response mRNAs are good candidates for these modes of sRNA regulation (Beisel and Storz, 2011; Massé and Gottesman, 2002; Vanderpool and Gottesman, 2004). Catalytic degradation, because it does not alter the total sRNA pool, could be the superior mode of regulation when a target mRNA exists in high copy numbers and requires a large dynamic range for function, or when a target mRNA needs to be fully repressed even under conditions of low sRNA levels. The MicM (ChiX) target *ybfM* (*chiP*) fits this scenario. *ybfM* (*chiP*) is completely silenced by MicM (ChiX) in the absence of chitooligosaccharide inducers (Figueroa-Bossi et al., 2009; Overgaard et al., 2009).

The coupled degradation mechanism is notable because it provides a threshold-linear response: regulation depends on the relative sRNA to mRNA ratio (Levine et al., 2007). Specifically, in the low sRNA:target mRNA regime, mRNA repression is not efficient because the sRNA is degraded following base-pairing and this greatly reduces the sRNA pool. Thus, coupled degradation is an excellent mechanism for rapidly turning over and thus eliminating the sRNA pool once the response is complete. Good examples for this case include the sRNAs RyhB and MicM (ChiX) (Figueroa-Bossi et al., 2009; Massé et al., 2003; Overgaard et al., 2009; Plumbridge et al., 2014).

Sequestration is an excellent mechanism for regulation of target mRNAs that require modulation rather than dramatic on-off changes. In this case, the mRNA levels are not significantly affected by sRNA regulation, which has the advantage of fine-tuning target expression levels. One example to consider is the sRNA Spot42 and its target *galK*. Spot42-directed repression of *galK* by sequestration presumably fine-tunes the relative levels of the galactose catabolism proteins for optimal carbon utilization (Møller et al., 2002). We hypothesize that the propensity for a target mRNA to sequester an sRNA depends on both the binding strength of the sRNA-mRNA pair and the degradation rate of the target mRNA upon pairing. Strong sequestration will occur if the target mRNA binds tightly to the sRNA but the target mRNA is not degraded efficiently. This is the case for the *luxO*-Qrr pair.

Finally, we show that the Qrr sRNA is degraded following activation of the *aphA* mRNA. We hypothesize that this mode of action generates a negative feedback loop that has the advantage of preventing overexpression of the target mRNA when the sRNA level is low. Specifically, because the sRNA is degraded during regulation, it cannot be reused. Thus, when the sRNA:target mRNA ratio is low, the degree of target mRNA activation is limited by the concentration of the sRNA.

Here, we rationalize the Qrr sRNAs use of particular regulatory mechanisms for the particular quorum-sensing target mRNAs. First, regarding *luxR* mRNA: LuxR is the master quorum-sensing regulator that, at high cell density, controls the bulk of genes in the quorum-sensing regulon (~600 genes in *V. harveyi*) (Rutherford et al., 2011). Our measurements of *luxR* mRNA and LuxR protein copy numbers indicate that *luxR* exists in high copy numbers (at least 40 mRNA copies and ~600 protein dimers per cell) at high cell density, presumably due to the requirement for LuxR dimers to bind their 115 DNA promoter sites (van Kessel et al., 2013; Teng et al., 2010). However, this high LuxR concentration presents a conundrum for the cell when it needs to, essentially instantaneously, transition to the low-cell-density mode upon, for example, excretion from the host or exit from a biofilm. Repression of *luxR* mRNA via a Qrr catalytic mechanism should be the most effective means to rapidly decrease high levels of LuxR protein to reset the quorum-sensing genetic program. Regarding *luxO* mRNA, which is controlled by a Qrr feedback-sequestration mechanism: the Qrr-to-*luxO* feedback loop acts as a rheostat to moderately adjust Qrr levels (Tu et al., 2010). We argue that using sequestration to regulate *luxO* mRNA prevents dramatic spikes and valleys in Qrr levels, while simultaneously buffering LuxO protein levels from valleys and spikes due to noise associated with fluctuations in Qrr levels. With respect to the use of coupled degradation to regulate *luxM* mRNA: we propose that the *luxM* mRNA and seven other target mRNAs that are able to base-pair with SL1 of the Qrr sRNAs (Shao et al., 2013) are exploited to control Qrr turnover in order to set the appropriate concentration of the total Qrr sRNA pool under different quorum-sensing states. This feature is important for when the cells initiate the high-cell-density program and they need to eliminate the Qrr sRNAs. Finally, as we discussed above, activation of *aphA* with concomitant degradation of the Qrr sRNAs may prevent overproduction of the AphA protein. Our finding that AphA protein production changes only 4- to 6-fold supports this hypothesis (Figure 7A). AphA fine-tunes quorum-sensing gene expression at low cell density (van Kessel et al., 2012). Keeping AphA levels in check may be critical for its subtle function. Indeed, AphA feeds back to repress Qrr transcription, which further guarantees tight control of AphA levels (Rutherford et al., 2011).

We predict that the regulatory mechanisms we discovered between Qrr3 and the target mRNAs are conserved across all five Qrr sRNAs based on their highly similar secondary structures and sequences (Tu and Bassler, 2007). The caveat is that Qrr1 lacks nine nucleotides in the first stem-loop, which makes it unable to regulate certain targets, such as *aphA* (Shao and Bassler, 2012). The five Qrr sRNAs are expressed at different levels and with somewhat different timing (Tu and Bassler, 2007). Thus, how the in vivo competition occurs between all five Qrr sRNAs and all 20 mRNA targets to provide a robust quorum-sensing response remains to be defined. Nonetheless, embedding the capacity for multiple regulatory mechanisms into a single sRNA is an evolutionarily economical method to endow a biological circuit with diverse dynamic behaviors. The principles underpinning the regulatory mechanisms we discovered here could be employed by other natural systems or to engineer synthetic sRNAs with numerous functions.

EXPERIMENTAL PROCEDURES

Strains, plasmids, and oligonucleotides used in this study are listed in Tables S1, S2, and S3. Detailed protocols are described in Extended Experimental Procedures.

Competition Assay

Overnight cultures (Table S1) were diluted 1,000-fold into fresh M9 minimal medium containing 0.5% glycerol, appropriate antibiotics, 0.2 mM IPTG,

0 or 3 ng ml^{-1} anhydrotetracycline (aTc; Clontech), and varying amounts of arabinose. GFP and mCherry fluorescence were measured following 10 hr of growth using fluorescence-activated cell sorting (FACS) (BD Biosciences FACSAria cell sorter).

RNA Expression and Half-Life

Qrr3 and target mRNAs were induced for 10 hr and measured by Northern blot to determine expression. Rifampicin (250 μg ml^{-1}) was added to stop transcription followed by collection of RNA at different time points to determine half-life.

V. harveyi GFP Assay

Overnight cultures of *V. harveyi* strains LF1838, LF1845, LF1848, LF2328, LF2332, and LF2335 were diluted to OD_{600} = 0.0002 into fresh AB medium containing 1 μM AI-1 and grown for 6.5 hr. 3-oxo-C12-HSL (100 μM; Sigma) (LuxN/AI-1 antagonist) was added to cultures. GFP and mCherry fluorescence were measured every 40 min thereafter using FACS.

Quantitative RT-PCR of *luxR* mRNA

Overnight cultures of *V. harveyi* strains LF2269, LF2246, and LF2254 were diluted into fresh LM medium to OD_{600} = 0.005 and grown for 6 hr to OD_{600} = 2.0. Cultures were diluted again into fresh LM medium to OD_{600} = 0.005. Total RNA was collected at 45, 90, 135, 180, and 345 min after the dilution. Total RNA (4 μg) was used for cDNA synthesis and quantitative RT-PCR (qRT-PCR) was performed as described in Supplemental Information.

qRT-PCR and Proteomics

Overnight cultures of *V. harveyi* strain TL25 were diluted 1:1,000-fold into fresh LM medium and grown to mid-log phase. Cultures were divided in half, and one aliquot was treated with 10 μM AI-1. Total RNA was collected from both samples at 0, 10, 20, 30, 40, 50, 60, and 90 min thereafter. Total RNA (4 μg) was used for cDNA synthesis and qRT-PCR was performed as described in Supplemental Information. Proteomics was performed as described in Supplemental Information.

SUPPLEMENTAL INFORMATION

Supplemental Information includes Extended Experimental Procedures, seven figures, and five tables and can be found with this article online at http://dx.doi.org/10.1016/j.cell.2014.11.051.

AUTHOR CONTRIBUTIONS

L.F., S.T.R., K.P., J.D.B., J.C.V.K., D.A.T., N.S.W., and B.L.B. designed the experiments. L.F., K.P., J.D.B., and J.C.V.K. performed the experiments. L.F., K.P., J.D.B., N.S.W., and B.L.B. analyzed the data. L.F., N.S.W., and B.L.B. wrote the paper.

ACKNOWLEDGMENTS

We thank Terence Hwa for generously providing the BW-RI strain and the pZA31-lucNB and pZE12G plasmids. We are indebted to members of the B.L.B. and N.S.W. laboratories for insightful discussions and suggestions. This work was supported by the Howard Hughes Medical Institute, NIH grant 5R01GM065859 and National Science Foundation (NSF) grant MCB-0343821 to B.L.B., NIH grant R01GM082938 to N.S.W., and NIH grant R01GM062523 and the Institute for Collaborative Biotechnologies through grant W911NF-09-0001 from the U.S. Army Research Office to D.A.T. K.P. is supported by a postdoctoral fellowship from the Human Frontiers in Science Program (HFSP). S.T.R. was supported by NIH fellowship F32AI085922. J.C.V.K. is supported by funds from Indiana University.

Received: May 2, 2014
Revised: September 20, 2014
Accepted: November 14, 2014
Published: January 8, 2015

REFERENCES

Altuvia, S., Zhang, A., Argaman, L., Tiwari, A., and Storz, G. (1998). The Escherichia coli OxyS regulatory RNA represses fhlA translation by blocking ribosome binding. EMBO J. *17*, 6069–6075.

Beisel, C.L., and Storz, G. (2011). The base-pairing RNA spot 42 participates in a multioutput feedforward loop to help enact catabolite repression in Escherichia coli. Mol. Cell *41*, 286–297.

Belasco, J.G. (2010). All things must pass: contrasts and commonalities in eukaryotic and bacterial mRNA decay. Nat. Rev. Mol. Cell Biol. *11*, 467–478.

Chatterjee, J., Miyamoto, C.M., and Meighen, E.A. (1996). Autoregulation of luxR: the Vibrio harveyi lux-operon activator functions as a repressor. Mol. Microbiol. *20*, 415–425.

Fender, A., Elf, J., Hampel, K., Zimmermann, B., and Wagner, E.G.H. (2010). RNAs actively cycle on the Sm-like protein Hfq. Genes Dev. *24*, 2621–2626.

Figueroa-Bossi, N., Valentini, M., Malleret, L., Fiorini, F., and Bossi, L. (2009). Caught at its own game: regulatory small RNA inactivated by an inducible transcript mimicking its target. Genes Dev. *23*, 2004–2015.

Fröhlich, K.S., and Vogel, J. (2009). Activation of gene expression by small RNA. Curr. Opin. Microbiol. *12*, 674–682.

Gottesman, S. (2004). The small RNA regulators of Escherichia coli: roles and mechanisms*. Annu. Rev. Microbiol. *58*, 303–328.

Hussein, R., and Lim, H.N. (2011). Disruption of small RNA signaling caused by competition for Hfq. Proc. Natl. Acad. Sci. USA *108*, 1110–1115.

Kawamoto, H., Koide, Y., Morita, T., and Aiba, H. (2006). Base-pairing requirement for RNA silencing by a bacterial small RNA and acceleration of duplex formation by Hfq. Mol. Microbiol. *61*, 1013–1022.

Lenz, D.H., Mok, K.C., Lilley, B.N., Kulkarni, R.V., Wingreen, N.S., and Bassler, B.L. (2004). The small RNA chaperone Hfq and multiple small RNAs control quorum sensing in Vibrio harveyi and Vibrio cholerae. Cell *118*, 69–82.

Levine, E., Zhang, Z., Kuhlman, T., and Hwa, T. (2007). Quantitative characteristics of gene regulation by small RNA. PLoS Biol. *5*, e229.

Long, T., Tu, K.C., Wang, Y., Mehta, P., Ong, N.P., Bassler, B.L., and Wingreen, N.S. (2009). Quantifying the integration of quorum-sensing signals with single-cell resolution. PLoS Biol. *7*, e1000068.

Majdalani, N., Cunning, C., Sledjeski, D., Elliott, T., and Gottesman, S. (1998). DsrA RNA regulates translation of RpoS message by an anti-antisense mechanism, independent of its action as an antisilencer of transcription. Proc. Natl. Acad. Sci. USA *95*, 12462–12467.

Massé, E., and Gottesman, S. (2002). A small RNA regulates the expression of genes involved in iron metabolism in Escherichia coli. Proc. Natl. Acad. Sci. USA *99*, 4620–4625.

Massé, E., Escorcia, F.E., and Gottesman, S. (2003). Coupled degradation of a small regulatory RNA and its mRNA targets in Escherichia coli. Genes Dev. *17*, 2374–2383.

McCullen, C.A., Benhammou, J.N., Majdalani, N., and Gottesman, S. (2010). Mechanism of positive regulation by DsrA and RprA small noncoding RNAs: pairing increases translation and protects rpoS mRNA from degradation. J. Bacteriol. *192*, 5559–5571.

Møller, T., Franch, T., Udesen, C., Gerdes, K., and Valentin-Hansen, P. (2002). Spot 42 RNA mediates discoordinate expression of the E. coli galactose operon. Genes Dev. *16*, 1696–1706.

Moon, K., and Gottesman, S. (2011). Competition among Hfq-binding small RNAs in Escherichia coli. Mol. Microbiol. *82*, 1545–1562.

Overgaard, M., Johansen, J., Møller-Jensen, J., and Valentin-Hansen, P. (2009). Switching off small RNA regulation with trap-mRNA. Mol. Microbiol. *73*, 790–800.

Papenfort, K., Bouvier, M., Mika, F., Sharma, C.M., and Vogel, J. (2010). Evidence for an autonomous 5′ target recognition domain in an Hfq-associated small RNA. Proc. Natl. Acad. Sci. USA *107*, 20435–20440.

Papenfort, K., Sun, Y., Miyakoshi, M., Vanderpool, C.K., and Vogel, J. (2013). Small RNA-mediated activation of sugar phosphatase mRNA regulates glucose homeostasis. Cell *153*, 426–437.

Plumbridge, J., Bossi, L., Oberto, J., Wade, J.T., and Figueroa-Bossi, N. (2014). Interplay of transcriptional and small RNA-dependent control mechanisms regulates chitosugar uptake in Escherichia coli and Salmonella. Mol. Microbiol. *92*, 648–658.

Prévost, K., Desnoyers, G., Jacques, J.-F., Lavoie, F., and Massé, E. (2011). Small RNA-induced mRNA degradation achieved through both translation block and activated cleavage. Genes Dev. *25*, 385–396.

Rutherford, S.T., and Bassler, B.L. (2012). Bacterial quorum sensing: its role in virulence and possibilities for its control. Cold Spring Harb. Perspect. Med. *2*, 1–25.

Rutherford, S.T., van Kessel, J.C., Shao, Y., and Bassler, B.L. (2011). AphA and LuxR/HapR reciprocally control quorum sensing in vibrios. Genes Dev. *25*, 397–408.

Shao, Y., and Bassler, B.L. (2012). Quorum-sensing non-coding small RNAs use unique pairing regions to differentially control mRNA targets. Mol. Microbiol. *83*, 599–611.

Shao, Y., Feng, L., Rutherford, S.T., Papenfort, K., and Bassler, B.L. (2013). Functional determinants of the quorum-sensing non-coding RNAs and their roles in target regulation. EMBO J. *32*, 2158–2171.

Storz, G., Vogel, J., and Wassarman, K.M. (2011). Regulation by small RNAs in bacteria: expanding frontiers. Mol. Cell *43*, 880–891.

Teng, S.-W., Wang, Y., Tu, K.C., Long, T., Mehta, P., Wingreen, N.S., Bassler, B.L., and Ong, N.P. (2010). Measurement of the copy number of the master quorum-sensing regulator of a bacterial cell. Biophys. J. *98*, 2024–2031.

Teng, S.-W., Schaffer, J.N., Tu, K.C., Mehta, P., Lu, W., Ong, N.P., Bassler, B.L., and Wingreen, N.S. (2011). Active regulation of receptor ratios controls integration of quorum-sensing signals in Vibrio harveyi. Mol. Syst. Biol. *7*, 491.

Tu, K.C., and Bassler, B.L. (2007). Multiple small RNAs act additively to integrate sensory information and control quorum sensing in Vibrio harveyi. Genes Dev. *21*, 221–233.

Tu, K.C., Waters, C.M., Svenningsen, S.L., and Bassler, B.L. (2008). A small-RNA-mediated negative feedback loop controls quorum-sensing dynamics in Vibrio harveyi. Mol. Microbiol. *70*, 896–907.

Tu, K.C., Long, T., Svenningsen, S.L., Wingreen, N.S., and Bassler, B.L. (2010). Negative feedback loops involving small regulatory RNAs precisely control the Vibrio harveyi quorum-sensing response. Mol. Cell *37*, 567–579.

Udekwu, K.I., Darfeuille, F., Vogel, J., Reimegård, J., Holmqvist, E., and Wagner, E.G.H. (2005). Hfq-dependent regulation of OmpA synthesis is mediated by an antisense RNA. Genes Dev. *19*, 2355–2366.

van Kessel, J.C., Rutherford, S.T., Shao, Y., Utria, A.F., and Bassler, B.L. (2012). The master regulators AphA and LuxR control the Vibrio harveyi quorum-sensing regulon: analysis of their individual and combined effects. J. Bacteriol. *195*, 436–443.

van Kessel, J.C., Ulrich, L.E., Zhulin, I.B., and Bassler, B.L. (2013). Analysis of activator and repressor functions reveals the requirements for transcriptional control by LuxR, the master regulator of quorum sensing in Vibrio harveyi. MBio. *4*, e00378-13.

Vanderpool, C.K., and Gottesman, S. (2004). Involvement of a novel transcriptional activator and small RNA in post-transcriptional regulation of the glucose phosphoenolpyruvate phosphotransferase system. Mol. Microbiol. *54*, 1076–1089.

Vogel, J., and Luisi, B.F. (2011). Hfq and its constellation of RNA. Nat. Rev. Microbiol. *9*, 578–589.

Wagner, E.G.H. (2013). Cycling of RNAs on Hfq. RNA Biol. *10*, 619–626.

Waters, L.S., and Storz, G. (2009). Regulatory RNAs in bacteria. Cell *136*, 615–628.

EXTENDED EXPERIMENTAL PROCEDURES

Bacterial Strains and Growth Conditions

E. coli strains S17-1λ*pir* (de Lorenzo and Timmis, 1994), DH10B (Invitrogen), BW-RI (Levine et al., 2007), and derivatives were grown aerobically in LB medium or in M9 minimal medium (0.5% glucose or 0.5% glycerol) at 37°C. All *V. harveyi* strains were derived from *V. harveyi* BB120 (BAA-1116) (Bassler et al., 1997) and grown aerobically at 30°C in either Luria-Marine (LM) broth or Autoinducer Bioassay (AB) broth. Antibiotics (Sigma-Aldrich) were used at the following concentrations: 50 U ml^{-1} polymyxin B (Pb), 100 μg ml^{-1} ampicillin (Amp), 100 μg ml^{-1} kanamycin (Kan), 10 μg ml^{-1} chloramphenicol (Cm), and 60 μg ml^{-1} spectinomycin (Spec). Plasmids were introduced into electrocompetent *E. coli* S17-1λ*pir*, DH10B, and BW-RI using 0.1 cm gap cuvettes (USA Scientific) and a Bio-Rad MicroPulser. Lists of strains and plasmids used in this study are provided in Tables S1 and S2.

DNA Manipulations and Strain Construction

E. coli S17-1λpir was used for regular cloning and strain DH10B was used for constructing plasmids containing point mutations, deletions, and insertions. DNA manipulations were performed as in Sambrook et al. (1989). iProof DNA polymerase (Bio-Rad) was used for regular PCR reactions, and pfu Ultra DNA polymerase (Agilent) was used for constructing point mutations, deletions, and insertions. Restriction enzymes, T4 DNA ligase, T4 polynucleotide kinase, and Antarctic phosphatase were purchased from New England Biolabs. Primers are listed in Table S3 and came from Integrated DNA Technologies (IDT). All plasmids were confirmed by sequencing at Genewiz.

The 5′UTRs of *luxR*, *luxO*, *luxM*, and *aphA* (see primers in Table S3) were blunt cloned under the PL*lac*-O1 promoter of plasmid pZE12G (Levine et al., 2007), generating pLF128, pLF129, pLF254, pLF255, respectively.

The Amp resistance gene from pBAD myc/His A (Invitrogen) was replaced with the Kan resistance gene using primers LF161-LF164 (Table S3), generating pBAD myc/His A-Kan. The *mCherry* gene was cloned downstream of the pBAD promoter and the ribosome binding site (control RBS) of pBAD myc/His A-Kan using primers LF173-LF176 (Table S3), yielding pLF343. The 5′UTRs of *luxM, luxO, luxR*, or *aphA* were blunt cloned under the pBAD promoter of pLF343. The *araC*-pBAD-target2 (including control RBS, *luxM* 5′UTR, *luxO* 5′UTR, *luxR* 5′UTR or *aphA* 5′UTR)-*mCherry* sequences were transferred to pLF128 using primers LF199, LF200, LF206, and LF207, yielding pLF518, pLF521, pLF523, pLF519, and pLF1481. Similar methods were used to generate pZE12G-*luxO-gfp*-target2-*mCherry* fusions. The stop codon in *mCherry* was introduced using primers LF215 and LF216, generating pLF507 and pLF537, respectively. The *araC*-pBAD-target2 (including *luxR* 5′UTR and *luxM* 5′UTR)-*mCherry** sequences were transferred to pLF128 to generate pLF2336 and pLF2338, respectively.

The *mCherry* gene was deleted from pZE12G-*luxO-gfp-luxM-mCherry* and pZE12G-*luxO-gfp-luxR-mCherry* using primers LF993-LF995 to generate pZE12G-*luxO-gfp-luxM* miniRNA and pZE12G-*luxO-gfp-luxR* miniRNA, respectively. Mutations in *luxM* miniRNA (changing UUGACCC (−8 to −2 relative to the translation start site) to GUCUGGG and changing CAUAAA (−24 to −19 relative to the translation start site) to GUCAG) and *luxR* miniRNA (changing AAAAA (−10 to −6 relative to the translation start site) to UGACCC and deleting CAACUCA (−27 to −21 relative to the translation start site)) were introduced using primers listed in Table S3, generating pZE12G-*luxO-gfp-luxM* $^{SL1,2\ to\ SL2}$ miniRNA and pZE12G-*luxO-gfp-luxR* $^{SL2\ to\ SL1,2}$ miniRNA, respectively. The *mCherry* gene was subsequently reintroduced into these two plasmids using primers LF1107-LF1111, yielding pZE12G-*luxO-gfp-luxM* $^{SL1,2\ to\ SL2}$-*mCherry* and pZE12G-*luxO-gfp-luxR* $^{SL2\ to\ SL1,2}$-*mCherry*, respectively.

The *araC*-pBAD-target2 (including *luxM* miniRNA, *luxR* miniRNA, *luxM* $^{SL1,2\ to\ SL2}$ miniRNA, *luxR* $^{SL2\ to\ SL1,2}$ miniRNA, *luxM* $^{SL1,2\ to\ SL2}$-*mCherry* or *luxR* $^{SL2\ to\ SL1,2}$-*mCherry*) sequences were transferred to pLF128 in similar ways as described above, generating pLF2197, pLF2199, pLF2200, pLF2202, pLF2204, and pLF2205, respectively. The *luxR*^{binding} mutation was introduced to pLF507 using primers LF1186, LF1187, yielding pLF2207.

The PL*lac*-O1-target (*luxR*, *luxO*, *luxM*)-*gfp* fusion sequences from pLF128, pLF129 and pLF254, respectively, together with a Cm resistance marker were integrated between the λ terminator and the *moeB* gene on pTL83 (Long et al., 2009) using λ red recombineering in *E. coli* (Datsenko and Wanner, 2000). These steps generated pLF1825, pLF1826 and pLF1824, respectively.

The *luxR* R17C mutation was introduced onto a pLAFR2 cosmid containing a genomic fragment harboring *luxR* from *V. harveyi* by λ red recombineering in *E. coli* (Datsenko and Wanner, 2000). This procedure yielded pLF2238. The 5′ UTRs of *luxM* and *luxO* (from the transcriptional start sites to −1 relative to the translational start sites) were fused to the *luxR* gene containing the R17C mutation and integrated onto the same cosmid, yielding pLF2236 and pLF2232, respectively.

V. harveyi mutants were generated by conjugation with *E. coli* carrying the pLAFR cosmids. Mutant alleles were incorporated onto the *V. harveyi* genome by homologous recombination (Bassler et al., 1993). Antibiotic markers were removed using FLP-mediated recombination (Long et al., 2009).

qRT-PCR Analysis

*Repression of luxR-mCherry**

Overnight cultures of LF514 were diluted 1,000-fold into fresh M9 minimal medium containing 0.5% glycerol, appropriate antibiotics, 0.2 mM IPTG, 0 or 3 ng ml^{-1} anhydrotetracycline (aTc; Clontech) and varying amounts of arabinose. RNA was isolated after 10 hr of growth.

Expression Level of the Competitor mRNAs

Overnight cultures of *E. coli* strains (Table S1) were diluted 1,000-fold into fresh M9 minimal medium containing 0.5% glycerol, appropriate antibiotics, and 0.2% arabinose. RNA was isolated after 10 hr of growth.

RNA was isolated following the protocol from the QIAgen RNeasy Minikit with RNAprotect (QIAGEN). 100 ng of total RNA was used for cDNA synthesis. cDNA was synthesized using SuperScript III reverse transcriptase (Invitrogen). Real-time PCR analyses were performed as described (Tu and Bassler, 2007) on an ABI Prism 7900HT Sequence Detection System using the Sybr Green mix (ABI). 5S rRNA was used as the internal control. The primers used for qRT-PCR are listed in Table S3.

Northern Blot Analysis

Qrr3 Production and Half-Life

Overnight cultures were diluted to OD_{600} = 0.02 in M9 minimal medium containing 0.5% glycerol, appropriate antibiotics, 3 ng ml^{-1} (1.5 ng ml^{-1} for Figure S3F) aTc, and 0.2% arabinose. To measure the *qrr*3 expression, total RNA was isolated after 10 hr of growth. To measure the Qrr3 half-life, 250 μg ml^{-1} rifampicin was added to stop transcription followed by collection of culture at different time points.

Target Expression Level

Overnight cultures were diluted 1:1,000-fold in M9 minimal medium containing 0.5% glucose, appropriate antibiotics, 0.5 mM IPTG, 0 or 6.25 ng ml^{-1} aTc. Total RNA was isolated when the OD_{600} reached 0.2 (approximately 10 hr).

miniRNA Expression Level

Overnight cultures of *E. coli* strains LF2176, LF2179, LF2182, LF2185 were diluted to OD_{600} = 0.02 in M9 minimal medium containing 0.5% glycerol, appropriate antibiotics, and 0.2% arabinose. Total RNA was isolated after 8 hr of growth. miniRNAs were detected using 5′ end-^{32}P-labeled oligonucleotide probes (Table S3 LF1113).

Qrr3 Half-Life in V. harveyi

Overnight cultures of *V. harveyi* strain KT282 harboring a plasmid with an arabinose-inducible *qrr*3, *qrr*3 $SL1_{mut}$ or *qrr*3 $SL1_{restore}$ were diluted 1:1,000 in fresh LM medium with 0.2% arabinose. 250 μg ml^{-1} rifampicin was added to terminate transcription when the cells had reached OD_{600} = 1.0. Aliquots of the culture were collected at different times thereafter.

Total RNA was isolated using phenol/chloroform extraction. Northern blots were carried out as previously described (Shao et al., 2013; Urban and Vogel, 2007). 5 mg of total RNA was resolved on 6% (for Qrr and miniRNA detection) or 5% (for target-*gfp* mRNA detection) polyacrylamide gels (7 M urea) followed by transfer to Hybond-XL membranes (GE Healthcare). Riboprobes were used for Qrr3 and target-*gfp* mRNA detection. A 5′ end-labeled DNA probe was used for miniRNA and 5S RNA detection. Membranes were hybridized with Riboprobes at 68°C and washed in three steps with SSC wash buffers (2X, 1X, 0.5X, respectively) supplemented with 0.1% SDS. Membranes were hybridized with DNA probe at 42°C and washed in three steps with SSC wash buffers (5X, 1X, 0.5X, respectively) supplemented with 0.1% SDS. Blots were exposed to a PhosphorImager screen (GE Healthcare), scanned with Typhoon 9410 (GE Healthcare), and band intensities were quantified with Image J (http://imagej.nih.gov/ij/). Riboprobes were synthesized using ^{32}P-α-UTP following the MAXIscript kit (Ambion) protocol. The 5′ end-labeled DNA probe was synthesized using T4 polynucleotide kinase in the presence of ^{32}P-γ-ATP.

Primer Extension

Primer extension experiments were performed as described (Fröhlich et al., 2013). Briefly, 10 μg of total RNA was denatured in the presence of 1 pmol 5′ end-labeled primer (KPO-0913) at 70°C for 5 min and chilled on ice for 5 min. Next, 5 μl of reaction mix (3 μl 5X first strand buffer, 5 mM DTT, 0.5 mM each dATP, dGTP, dCTP and dTTP) was combined with the samples at 42°C, and 1 μl SuperScript III (200 U) was added. cDNA synthesis was performed at 50°C for 60 min, followed by incubation at 70°C for 15 min to inactivate the enzyme. Samples were treated with RNase H (1 μl; 2.5 U) for 15 min at 37°C and reactions were stopped by phenol/chloroform extraction. Samples were separated using electrophoresis on 6%–8% sequencing gels together with a template-specific cDNA ladder.

Proteomics

Relative rates of protein synthesis were measured by combining bio-orthogonal non-canonical amino acid tagging (BONCAT) and stable isotope labeling with amino acids in cell culture (SILAC) (Bagert et al., 2014). TL25 cultures were grown in AB medium supplemented either with standard "light" lysine or with "heavy" lysine (13C6, 99%; 15N2, 99%, Cambridge Isotope Laboratories, Inc.). Upon reaching mid-exponential phase (i.e., after approximately 5 cell doublings), one of the cultures was treated with 10 μM AI-1 (t = 0 min). Rates of protein synthesis were measured over 90 min, with each 10 min period analyzed in a separate experiment performed in triplicate. Newly synthesized proteins from each 10 min period were labeled by treating both light and heavy cultures with 1 mM azidohomoalanine (Aha), an analog of methionine. Protein synthesis was terminated 10 min after Aha addition by treating with chloramphenicol (Sigma-Aldrich) at a concentration of 100 μg ml^{-1}. Lysates from paired light and heavy SILAC cultures were mixed at equal concentrations of total protein. Aha-labeled proteins were conjugated to an acid-cleavable alkyne-biotin probe and purified with Streptavidin Plus UltraLink Resin (Thermo Scientific) (Szychowski et al., 2010). Purified proteins were separated by gel electrophoresis in NuPAGE 4%–12% Bis-Tris Protein Gels (Life Technologies), digested in-gel with LysC (Mako), extracted, and desalted with custom-packed C_{18} columns. Peptides were separated on an EASY-nLC (Thermo Scientific) in line with a nano-electrospray ion source and detected with a hybrid LTQ-Orbitrap (Thermo Scientific). Thermo RAW files were processed with MaxQuant (v. 1.4.1.2).

RNA Copy Number Measurement

Overnight cultures of *V. harveyi* strains TL25, LF1451, JS202 and JAF78 (Table S1) were diluted to OD_{600} = 0.001 in fresh LM medium and grown for 6 hr to OD_{600} = 1.5. Total RNA was isolated by following the protocol from the QIAgen RNeasy Minikit with RNAprotect

(QIAGEN). Serial dilutions of TL25 cells were plated on LM agar plates and grown in a 30°C incubator. CFU were counted the following day and the number of cells collected for RNA isolation was calculated.

DNA templates for *qrr*1, *qrr*2, *qrr*3, *qrr*4, *luxR* and *luxO* were generated using primers listed in Table S3. RNA was synthesized in vitro using the MEGAshortscript T7 kit (Ambion) (for Qrr1, Qrr2, Qrr3, Qrr4) or MEGAscript T7 kit (Ambion) (for *luxR* and *luxO*). In vitro transcribed RNAs were purified from 8% (for Qrr1, Qrr2, Qrr3, Qrr4) or 4.5% (for *luxR* and *luxO*) polyacrylamide gels (7 M urea) using the phenol/chloroform extraction method. RNAs were quantified using a Nanodrop (Thermo). For each RNA species, three independent in vitro transcription reactions were performed. Three independent RNA standards were generated for each RNA by adding 10^{12}, 10^{11}, 10^{10}, 10^{9}, 10^{8}, 10^{7}, 10^{6}, 10^{5} copies of in vitro transcribed RNA to 4 μg of the background RNA. For Qrr2, Qrr3, Qrr4, the background RNA used was the total RNA isolated from LF1451. For Qrr1 and *luxR*, the background RNA used was the total RNA isolated from JS202. For *luxO*, the background RNA used was the total RNA isolated from JAF78. 4 μg of total RNA from the RNA standards and from the TL25 RNA sample was used for cDNA synthesis. qRT-PCR was performed as described earlier. (Note: This method does not account for the loss of RNA during isolation, thus the copy number of each RNA species should be higher than what's measured here. However, for our modeling purpose, only the Qrr sRNA: target mRNA ratio matters, thus our results can still be used.)

Supplemental Information for Modeling

We begin by considering a particular cognate sRNA-mRNA pair competing for Hfq binding against a background of other cellular sRNAs and mRNAs. This situation is represented by Equations S1 and S2 below:

$$[\mathrm{sRNA}_i:\ \mathrm{Hfq}:\ \mathrm{mRNA}_j] = [\mathrm{Hfq}]_{\mathrm{total}} \frac{[\mathrm{sRNA}_i]_{\mathrm{free}}[\mathrm{mRNA}_j]_{\mathrm{free}}/K_{ij}}{\sum_{i'j'}[\mathrm{sRNA}_{i'}]_{\mathrm{free}}\left[\mathrm{mRNA}_{j'}\right]_{\mathrm{free}}/K_{i'j'}} \quad \text{(Equation S1)}$$

$$[\mathrm{Hfq}]_{\mathrm{total}} = \sum_{ij}[\mathrm{sRNA}_i : \mathrm{Hfq} : \mathrm{mRNA}_j]. \quad \text{(Equation S2)}$$

The kinetic equations for each sRNA and mRNA species are:

$$\frac{d[\mathrm{sRNA}_i]}{dt} = \Gamma_{\mathrm{sRNA}_i} - \gamma_{si}[\mathrm{sRNA}_i]_{\mathrm{free}} - \sum_j \gamma^E_{si,j}[\mathrm{sRNA}_i:\ \mathrm{Hfq}:\ \mathrm{mRNA}_j] \quad \text{(Equation S3)}$$

$$\frac{d[\mathrm{mRNA}_j]}{dt} = \Gamma_{\mathrm{mRNA}_j} - \gamma_j[\mathrm{mRNA}_j]_{\mathrm{free}} - \sum_i \gamma^E_{i,j}[\mathrm{sRNA}_i:\ \mathrm{Hfq}:\ \mathrm{mRNA}_j]. \quad \text{(Equation S4)}$$

The total concentrations of sRNA_i and mRNA_j are thus given by:

$$[\mathrm{sRNA}_i] = [\mathrm{sRNA}_i]_{\mathrm{free}} + \sum_j [\mathrm{sRNA}_i:\ \mathrm{Hfq}:\ \mathrm{mRNA}_j] \quad \text{(Equation S5)}$$

$$[\mathrm{mRNA}_j] = [\mathrm{mRNA}_j]_{\mathrm{free}} + \sum_i [\mathrm{sRNA}_i:\ \mathrm{Hfq}:\ \mathrm{mRNA}_j]. \quad \text{(Equation S6)}$$

In Equation S1, the concentration of a particular sRNA-mRNA pair complexed with Hfq is given by the total concentration of Hfq times the fraction bound by that pair. Since we assume different sRNA-mRNA pairs compete for Hfq binding, the fraction of Hfq bound to a particular pair, sRNA_i-mRNA_j, is given by the concentration of free sRNA_i times the concentration of free mRNA_j divided by the dissociation constant of the pair sRNA_i-mRNA_j from Hfq, and normalized by the sum in the denominator so as to yield Hfq saturation.

In Equations S3 and S4, Γ_{sRNA_i} and Γ_{mRNA_j} are the production rates of sRNA_i and mRNA_j. γ_{si} and γ_j are the degradation rates of free sRNA_i and mRNA_j, and $\gamma^E_{si,j}$ and $\gamma^E_{i,j}$ are the degradation rates of sRNA_i and mRNA_j when each is bound to Hfq together with mRNA_j or sRNA_i.

Model for One Qrr sRNA Regulating One mRNA Target

We first modeled the scenario in which one Qrr sRNA regulates one mRNA target. We use sRNA_0 and mRNA_0 to represent all the cellular sRNAs and mRNAs that bind to and compete for Hfq. sRNA_1 represents the Qrr sRNA and mRNA_1 represents the target mRNA. The resulting kinetic equations are:

$$\frac{d[\mathrm{mRNA}_j]}{dt} = \Gamma_{\mathrm{mRNA}_j} - \gamma_j[\mathrm{mRNA}_j]_{\mathrm{free}} - \gamma^E_{0,j}[\mathrm{sRNA}_0:\ \mathrm{Hfq}:\ \mathrm{mRNA}_j] - \gamma^E_{1,j}[\mathrm{sRNA}_1:\ \mathrm{Hfq}:\ \mathrm{mRNA}_j] \quad (j = 0, 1) \quad \text{(Equation S7)}$$

$$\frac{d[\mathrm{sRNA}_i]}{dt} = \Gamma_{\mathrm{sRNA}_i} - \gamma_{si}[\mathrm{sRNA}_i]_{\mathrm{free}} - \gamma^E_{si,0}[\mathrm{sRNA}_i{:}\ \ \mathrm{Hfq}:\ \ \mathrm{mRNA}_0] - \gamma^E_{si,1}[\mathrm{sRNA}_i{:}\ \ \mathrm{Hfq}:\ \ \mathrm{mRNA}_1] \quad (i = 0, 1). \qquad \text{(Equation S8)}$$

The total concentration of mRNA_0 [mRNA_0] is given by the sum of the concentration of free mRNA_0 species $[\mathrm{mRNA}_0]_{\mathrm{free}}$, the concentration of mRNA_0 bound to Hfq with sRNA_0 [sRNA_0: Hfq: mRNA_0] and the concentration of mRNA_0 bound to Hfq with sRNA_1 [sRNA_1: Hfq: mRNA_0] (Equation S6). Similar equations apply to mRNA_1, sRNA_0, and sRNA_1. The total concentration of Hfq protein is given by Equation S2 and the concentration of each specific sRNA_i:Hfq:mRNA_j complex is given by Equation S1.

We assume that the total concentrations of sRNAs and mRNAs in a cell are much larger than those of the Qrr sRNAs and its target mRNAs, thus Hfq is mainly saturated by other cellular sRNAs and mRNAs. In this limit, the denominator in Equation S1 can be approximated as $[\mathrm{sRNA}_0][\mathrm{mRNA}_0]/K_{0,0}$. At steady state, the kinetic Equations S7 and S8 must equal zero, and we analytically solved the resulting quadratic equation.

Our aim is to use the above equations to understand, at a qualitative level, how the different regulatory mechanisms affect sRNA regulatory efficacy. The parameters that dictate the specific regulatory mechanism are the degradation rates of sRNA and mRNA when they are in complex with Hfq ($\gamma^E_{S1,1}$ and $\gamma^E_{1,1}$). Therefore, we keep the rest of the parameters constant. For simplicity, we assume that mRNA binding to Hfq with a non-cognate sRNA does not affect the degradation rate of the mRNA, thus $\gamma^E_{0,0}$, $\gamma^E_{1,0}$ and $\gamma^E_{0,1}$ are set to the degradation rate of the free mRNA, γ_0 or γ_1. The half-life of the target mRNAs are 4-8 min (unpublished data), we chose γ_0 and γ_1 to be 0.25 min^{-1}. The half-life of Qrr sRNA in an Hfq mutant strain is about 5 min (unpublished data), so we chose γ_{S1} to be 0.2 min^{-1}. In the absence of Qrr targets, the half-life of the Qrr sRNA in a wild-type strain is over 32 min, so we set $\gamma^E_{S1,0}$ to be 0.03 min^{-1}. These parameter choices are consistent with the observation that Hfq protects the Qrr sRNAs from degradation (Lenz et al., 2004; unpublished data). For mRNA targets that are regulated by coupled degradation, the degradation rates of both the sRNA and the mRNA should be much larger when in a cognate sRNA-Hfq-mRNA complex than when free. Here we assume 100-fold faster degradation of sRNA when in the sRNA-Hfq-mRNA complex ($\gamma^E_{S1,1} = 3\ \mathrm{min}^{-1}$) and 16-fold faster degradation of mRNA when in the complex ($\gamma^E_{1,1} = 4\ \mathrm{min}^{-1}$). For mRNA targets that are regulated by catalytic degradation, the degradation rate of the mRNA in the sRNA-Hfq-mRNA complex $\gamma^E_{1,1}$ should also be much larger than that of the free mRNA, γ_1, so we set $\gamma^E_{1,1}$ to be 4 min^{-1}. The degradation rate of the sRNA in the sRNA-Hfq-mRNA complex should not be affected, thus $\gamma^E_{S1,1}$ remains at 0.03 min^{-1}. For mRNA targets that are regulated by sequestration, the degradation rates of both the mRNA and the sRNA should be the same when in the sRNA-Hfq-mRNA complex as when free, thus $\gamma^E_{1,1}$ is 0.25 min^{-1} and $\gamma^E_{S1,1}$ is 0.03 min^{-1}. K_d values for all nonspecific sRNA and mRNA pairs were set to be 1, which defines our unit of concentration. We assume a 100-fold higher binding energy, thus 100-fold smaller dissociation constant $K_{1,1}$ from Hfq, for the Qrr sRNA and its target mRNA compared to any other pairs. Hfq concentrations in *E. coli* are estimated to range from 400 to 10,000 hexamers per cell (Ali Azam et al., 1999; Carmichael et al., 1975; Kajitani et al., 1994). We chose the total concentration of Hfq to be 10,000 complexes per cell, though for qualitative comparison of the regulatory mechanisms this choice was arbitrary. The total concentrations of sRNA_0 and mRNA_0 were then set to be 10,000 per cell to satisfy the assumption that Hfq is saturated by cellular sRNAs and mRNAs. The copy number of Qrr mRNA targets should be much smaller compared to cellular mRNAs, thus the production rate of the Qrr mRNA target was chosen to be 10 copies/min/cell. The production rate of Qrr sRNA ranges from 0 (no Qrr) to 100 copies/min/cell (Qrr in excess compared to mRNA targets). We plotted the level of the translated mRNA and the level of total Qrr sRNA versus the production rate of the sRNA in Figure 5.

We next used Equations S7, S8, and S9, the kinetic equation for protein production, to study how different regulatory mechanisms affect the target dynamics during sRNA regulation. We examined the situation in which sRNA production was induced at time zero and terminated after two hours. The parameters are the same as we used to study regulatory efficacy above except we chose the production rate of Qrr sRNA to be 20 copies/min/cell. We assume the proteins are stable in the cell, thus the half-lives of the proteins are set by the dilution rate due to cell division. The doubling time of *V. harveyi* in LM is 40 min, thus the degradation rate of the protein is ln2/40 min^{-1} = 0.0075 min^{-1}. The initial conditions are: free Qrr: 0 copies per cell, free mRNA_1: 20 copies per cell, protein: 100 copies per cell. The production rate of the protein is chosen to agree with the initial protein copy number.

$$\frac{d[\mathrm{Protein}]}{dt} = \Gamma_p\left([\mathrm{mRNA}_1]_{\mathrm{free}} + [\mathrm{sRNA}_0{:}\ \ \mathrm{Hfq}:\ \ \mathrm{mRNA}_1]\right) - \gamma_p[\mathrm{Protein}]. \qquad \text{(Equation S9)}$$

Model for Competition between Two mRNA Targets

To explore how the different regulatory mechanisms affect the competition for sRNA regulation, we used Equations S1, S2, S3, S4, S5, and S6 to model the situation in which one sRNA regulates two mRNA targets. In our system, we have one target mRNA (mRNA_1) and one competitor mRNA (mRNA_2). We chose the target mRNA_1 to be regulated by a catalytic mechanism and the competitor mRNA_2 to be regulated either by sequestration, coupled degradation, or catalytic degradation. The equations are identical to those in the previous section except we added one mRNA species to the system. We solved the resulting cubic equation numerically using Matlab.

The degradation rates of the various mRNAs and sRNAs and the dissociation constants for the competitor mRNA_2:Hfq:sRNA_1 complexes are given in Table S4. The dissociation constant of the target mRNA_1:Hfq:sRNA_1 was set to be 0.1. We chose the production rate of the target mRNA (Γ_{mRNA_1}) to be 10 copies/min/cell and the production rate of sRNA (Γ_{sRNA_1}) to be 50 copies/min/cell. We subsequently varied the production rate of the competitor mRNA (Γ_{mRNA_2}) from 0 to 500 copies/min/cell. We plotted the

translated $mRNA_1$ level versus the production rate of $mRNA_2$ (Figure 5B). Our result shows that coupled degradation gives the most efficient competition: the level of translated $mRNA_1$ increases with the production rate of the competitor $mRNA_2$ and saturates when Γ_{mRNA_2} reaches approximately 150 copies/min/cell. Sequestration also leads to competition, but to a much lesser extent: the level of translated $mRNA_1$ also increases with the production rate of the competitor $mRNA_2$ but does not saturate even when Γ_{mRNA_2} reaches 500 copies/min/cell. Catalytic degradation barely competes.

Parameters for Conceptual Model of the V. harveyi *QS Circuit*

In Figure S7, we report measurements of the copy number of Qrr1-4, *luxR* mRNA, and *luxO* mRNA in strain locked in low-cell-density mode (Extended Experimental Procedures). We did not measure the copy number of Qrr5 since it is not functional in vivo (Tu and Bassler, 2007). From previous measurements, *luxR* mRNA level increases more than 10-fold (van Kessel et al., 2012) and *luxO* mRNA does not significantly change from low cell density to high cell density (Tu et al., 2010). Thus, the copy number of *luxR* mRNA at high cell density should be at least 4.4 × 10 = 44 copies/cell. *luxO* mRNA should remain at 1.3 copies/cell at high cell density. For convenience, we chose 60 copies/cell for *luxR* mRNA and 2 copies/cell for *luxO* mRNA.

We used the following parameters: The degradation rates of free *luxR* and *luxO* mRNA γ_{Rm} and γ_{Om} are 0.25 min^{-1} (Table S4). Since the *luxO* mRNA copy number is 2 copies per cell, the production rate of *luxO* mRNA Γ_{Om} is thus 2 × 0.25 = 0.5 copies/min. The *luxR* mRNA copy number is 60 copies per cell, thus the production rate of *luxR* mRNA Γ_{Rm} is 60 × 0.25 = 15 copies/min. We assume the LuxR and LuxO proteins are stable in the cell, thus the half-lives of the LuxR and LuxO proteins are set by the dilution rate due to cell division. The doubling time of *V. harveyi* in LM is 40 min, thus the degradation rates of LuxR and LuxO proteins γ_{Rp} and γ_{Op} are ln2 / 40 min^{-1} = 0.0075 min^{-1}. Based on previous measurements, the LuxR protein copy number is about 600 dimers per cell at high cell density (Teng et al., 2010). We chose 1,000 copies per cell for simplicity, thus the production rate of LuxR protein Γ_{Rp} is 1,000 × (1n2 / 40) / 60 = 0.29 min^{-1}. We do not know the copy number of LuxO protein inside the cell. We arbitrarily chose LuxO protein copy number to be 100 copies per cell, so the production rate Γ_{Op} is 100 × (1n2 / 40) / 2 = 0.87 min^{-1}. The degradation rate of free Qrr sRNA γ_{Qrr} is 0.2 min^{-1} as shown in Table S4. The Qrr sRNA copy number is 1,000 copies per cell based on our measurement (Figure S7). Thus, the production rate of Qrr sRNA, Γ_{Qrr}, is the copy number of Qrr × degradation rate of free Qrr / the copy number of phosphorylated LuxO, so Γ_{Qrr} = 1,000 × 0.2 / 100 = 2 min^{-1}. We take the dissociation constant for the Qrr-*luxO* pair from Hfq to be K_{QO} = 0.01. Since the binding energy of *luxR* to Qrr is weaker than that of *luxO* to Qrr (Figure 3A), we chose the dissociation constant for a Qrr-*luxR* pair from Hfq to be K_{QR} = 0.02. Since *luxO* is regulated by sequestration, the degradation rate of *luxO* mRNA when bound to Qrr and Hfq γ^E_{QO} is still 0.25 min^{-1} and the degradation rate of Qrr when bound to *luxO* and Hfq γ^E_{SQO} is 0.03 min^{-1} (Table S4). We examined three possible mechanisms for *luxR* regulation: catalytic, coupled degradation, and sequestration. The parameters for the degradation rate of *luxR* mRNA when bound to Qrr sRNA and Hfq γ^E_{QR} and the degradation rate of the Qrr sRNA when bound to *luxR* mRNA and Hfq γ^E_{SQR} for different mechanisms are the same as $\gamma^E_{1,1}$ and $\gamma^E_{S1,1}$ in Table S4.

SUPPLEMENTAL REFERENCES

Ali Azam, T., Iwata, A., Nishimura, A., Ueda, S., and Ishihama, A. (1999). Growth phase-dependent variation in protein composition of the Escherichia coli nucleoid. J. Bacteriol. *181*, 6361–6370.

Bagert, J.D., Xie, Y.J., Sweredoski, M.J., Qi, Y., Hess, S., Schuman, E.M., and Tirrell, D.A. (2014). Quantitative, time-resolved proteomic analysis by combining bioorthogonal noncanonical amino acid tagging and pulsed stable isotope labeling by amino acids in cell culture. Mol. Cell. Proteomics *13*, 1352–1358.

Bassler, B.L., Wright, M., Showalter, R.E., and Silverman, M.R. (1993). Intercellular signalling in Vibrio harveyi: sequence and function of genes regulating expression of luminescence. Mol. Microbiol. *9*, 773–786.

Bassler, B.L., Greenberg, E.P., and Stevens, A.M. (1997). Cross-species induction of luminescence in the quorum-sensing bacterium Vibrio harveyi. J. Bacteriol. *179*, 4043–4045.

Carmichael, G.G., Weber, K., Niveleau, A., and Wahba, A.J. (1975). The host factor required for RNA phage Qbeta RNA replication in vitro. Intracellular location, quantitation, and purification by polyadenylate-cellulose chromatography. J. Biol. Chem. *250*, 3607–3612.

Datsenko, K.A., and Wanner, B.L. (2000). One-step inactivation of chromosomal genes in Escherichia coli K-12 using PCR products. Proc. Natl. Acad. Sci. USA *97*, 6640–6645.

de Lorenzo, V., and Timmis, K.N. (1994). Analysis and construction of stable phenotypes in gram-negative bacteria with Tn5- and Tn10-derived minitransposons. Methods Enzymol. *235*, 386–405.

Fröhlich, K.S., Papenfort, K., Fekete, A., and Vogel, J. (2013). A small RNA activates CFA synthase by isoform-specific mRNA stabilization. EMBO J. *32*, 2963–2979.

Kajitani, M., Kato, A., Wada, A., Inokuchi, Y., and Ishihama, A. (1994). Regulation of the Escherichia coli hfq gene encoding the host factor for phage Q beta. J. Bacteriol. *176*, 531–534.

Sambrook, J., Fritsch, E.F., and Maniatis, T. (1989). Molecular Cloning: A Laboratory Manual (Cold Spring Harbor: Cold Spring Harbor Laboratory Press).

Szychowski, J., Mahdavi, A., Hodas, J.J.L., Bagert, J.D., Ngo, J.T., Landgraf, P., Dieterich, D.C., Schuman, E.M., and Tirrell, D.A. (2010). Cleavable biotin probes for labeling of biomolecules via azide-alkyne cycloaddition. J. Am. Chem. Soc. *132*, 18351–18360.

Urban, J.H., and Vogel, J. (2007). Translational control and target recognition by Escherichia coli small RNAs in vivo. Nucleic Acids Res. *35*, 1018–1037.

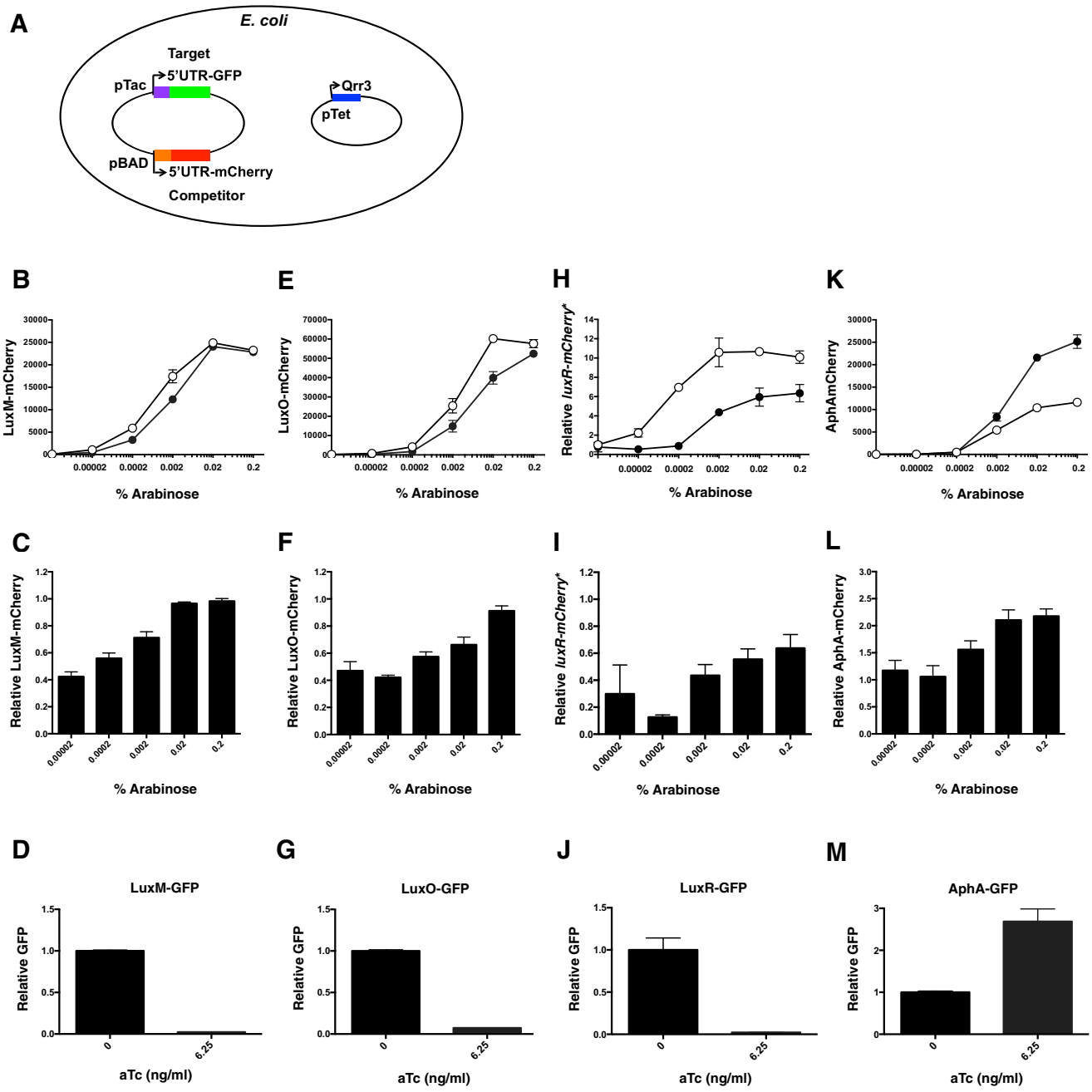

Figure S1. Regulation of Target mRNAs by Qrr3, Related to Figure 2

(A) Schematic of the competition assay.

(B, E, H, and K) Fluorescence was measured from LuxM-mCherry (B), LuxO-mCherry (E), AphA-mCherry (K) and mRNA was measured from *luxR-mCherry** (H) in the absence (open circles) and in the presence (filled circles) of Qrr3. Means and SEMs for triplicate cultures are shown. In (H), data were normalized to that from 0 arabinose in the absence of Qrr3.

(C, F, I, and L) mCherry fluorescence or mRNA measured in the presence of Qrr3 was normalized to that in its absence under the arabinose concentrations shown in (B), (E), (H), and (K), respectively. Means and SEMs for triplicate cultures are shown.

(D, G, J, and M) Fluorescence from LuxM-GFP (D), LuxO-GFP (G), LuxR-GFP (J), and AphA-GFP (M) translational fusions was measured in the absence (0 aTc) and in the presence (6.25 ng/ml aTc) of Qrr3. Means and SEMs for triplicate cultures are shown.

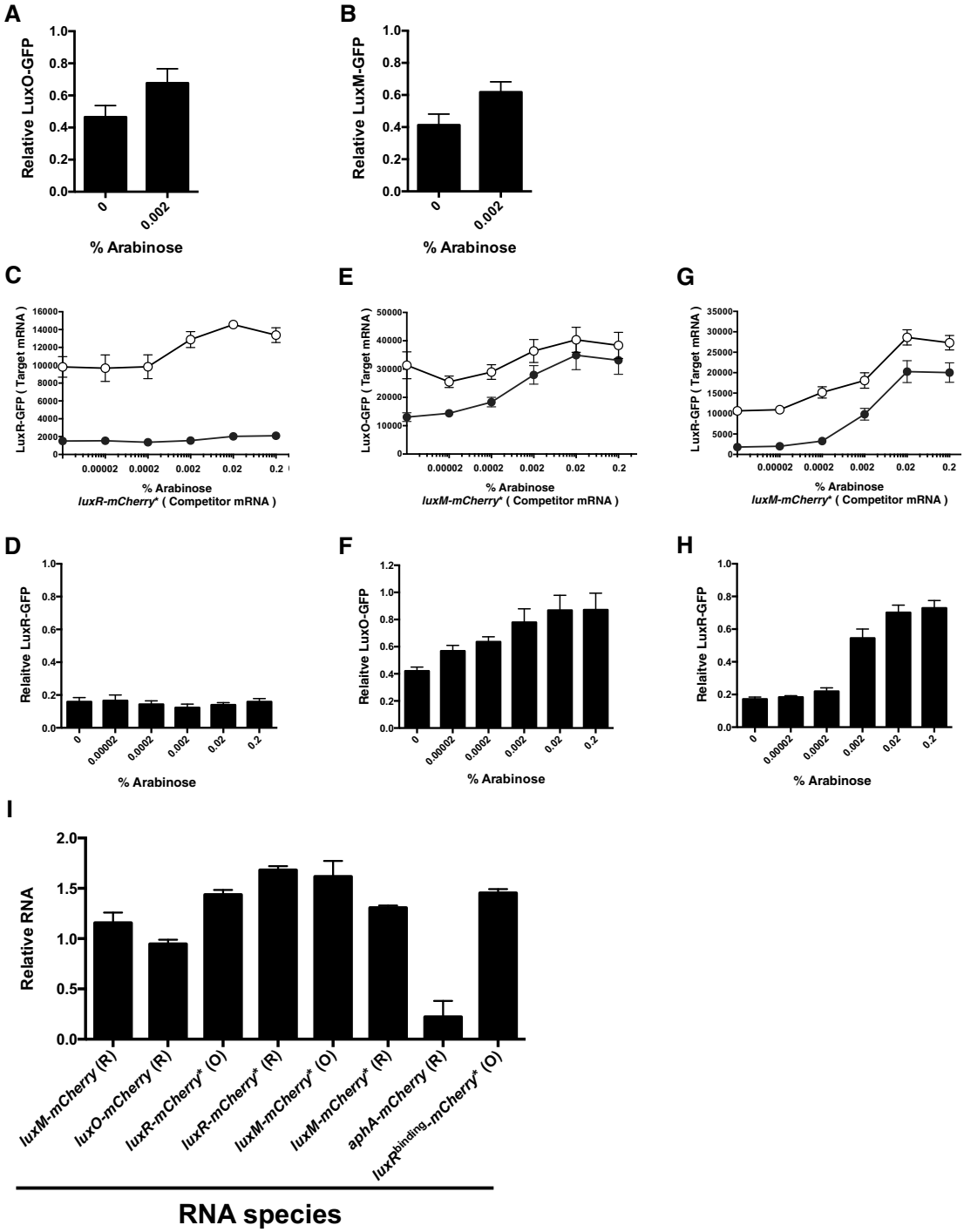

Figure S2. Control for the Competition Assay, Related to Figure 2

(A and B) Competition for Qrr3 regulation by *luxM-mCherry* mRNA against *luxO-gfp* (A) or *luxM-gfp* (B). Normalization as in Figure 2.

(C, E, and G) Fluorescence from plasmid-borne *luxR-gfp* (C and G) or *luxO-gfp* (E) was measured in *E. coli*. Arabinose was used to drive different levels of production of the competitor mRNA *luxR-mCherry** (C) or *luxM-mCherry** (E and G). Experiments were performed in the absence (open circles) and in the presence (filled circles) of Qrr3. Means and SEMs for triplicate cultures are shown.

(D, F, and H) Quantification of the fractional expression of LuxR-GFP (D and H) or LuxO-GFP (F) from (C), (G), and (E), respectively. GFP fluorescence in the presence of Qrr3 was normalized to that in its absence. Means and SEMs for triplicate cultures are shown.

(I) qRT-PCR of competitor mRNA levels. The letter in parentheses denotes the target mRNA ('O' for *luxO* and 'R' for *luxR*) that is harbored on the same plasmid as the competitor mRNA. Data were normalized to that from *luxM-mCherry*. Means and SEMs of three independent cultures are shown.

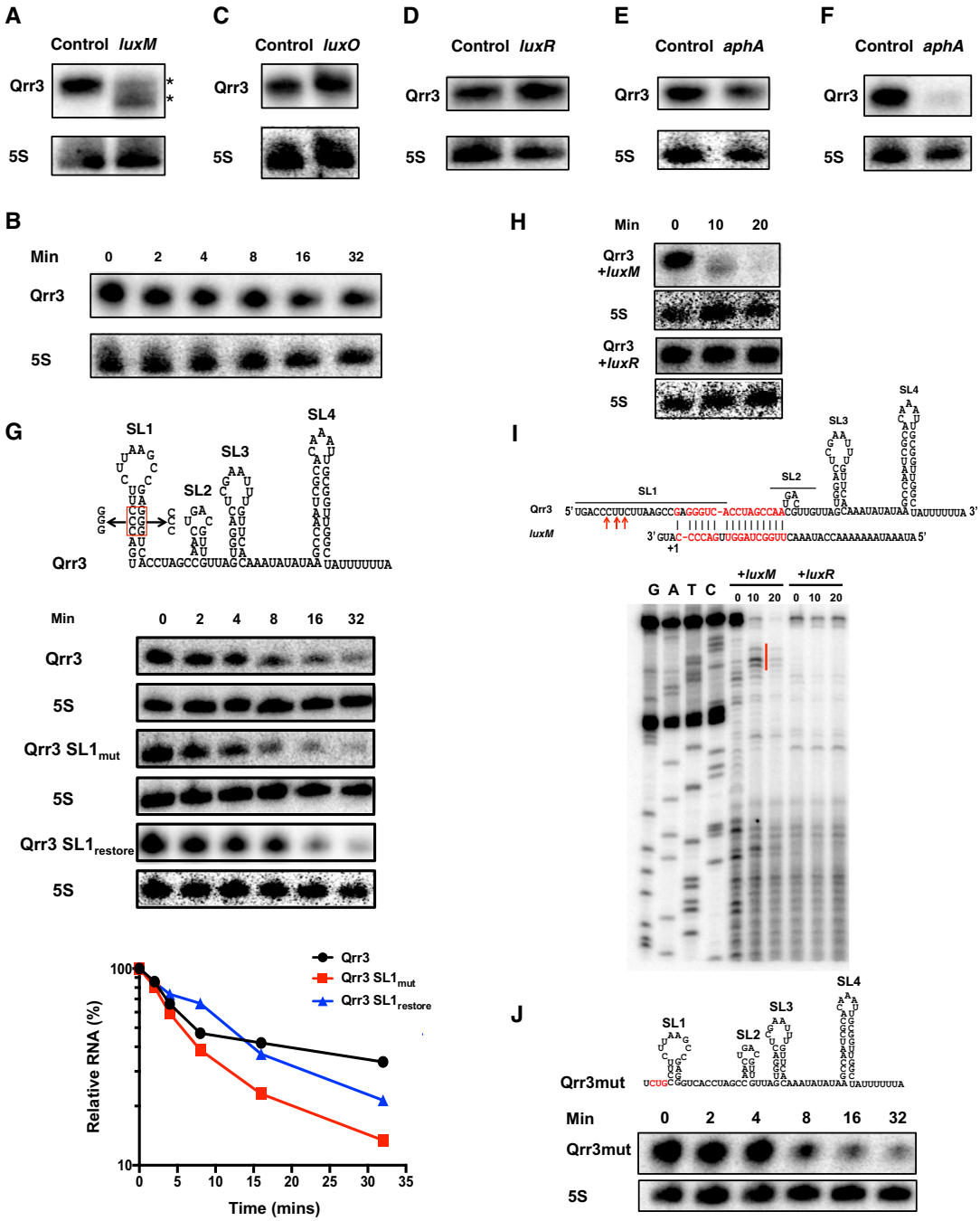

Figure S3. Target mRNAs Differentially Affect Qrr3 Levels, Related to Figures 2 and 3

(A, C, D, E, and F) Northern blots showing Qrr3 levels in the presence of a vector control and in the presence of a plasmid expressing arabinose inducible *luxM-mCherry* (A), *luxO-mCherry* (C), *luxR-mCherry* (D), and *aphA-mCherry* (E and F). Lower levels of Qrr3 were induced in (F) compared to (E) (see Extended Experimental Procedures).

(B) Northern blot showing the Qrr3 half-life in the absence of target mRNAs. Results are representative of two independent experiments.

(G) Half-lives of plasmid-encoded *V. harveyi* WT Qrr3 (pLF898), the SL1 disrupted Qrr3 mutant (Qrr3 SL1mut, pLF2360), and the corresponding SL1 restored Qrr3 mutant (Qrr3 SL1restore, pLF2378) were measured in *V. harveyi* strain KT282 by Northern analysis.

(H) Northern blot showing Qrr3 levels following induction of *luxM-mCherry* or *luxR-mCherry* mRNA with 0.2% arabinose at OD_{600} = 0.2. Results are representative of two independent experiments.

(I) Primer extension analysis showing the processing sites of the Qrr3 sRNA following induction of *luxM-mCherry* mRNA.

(J) Northern blot showing the Qrr3mut sRNA half-life.

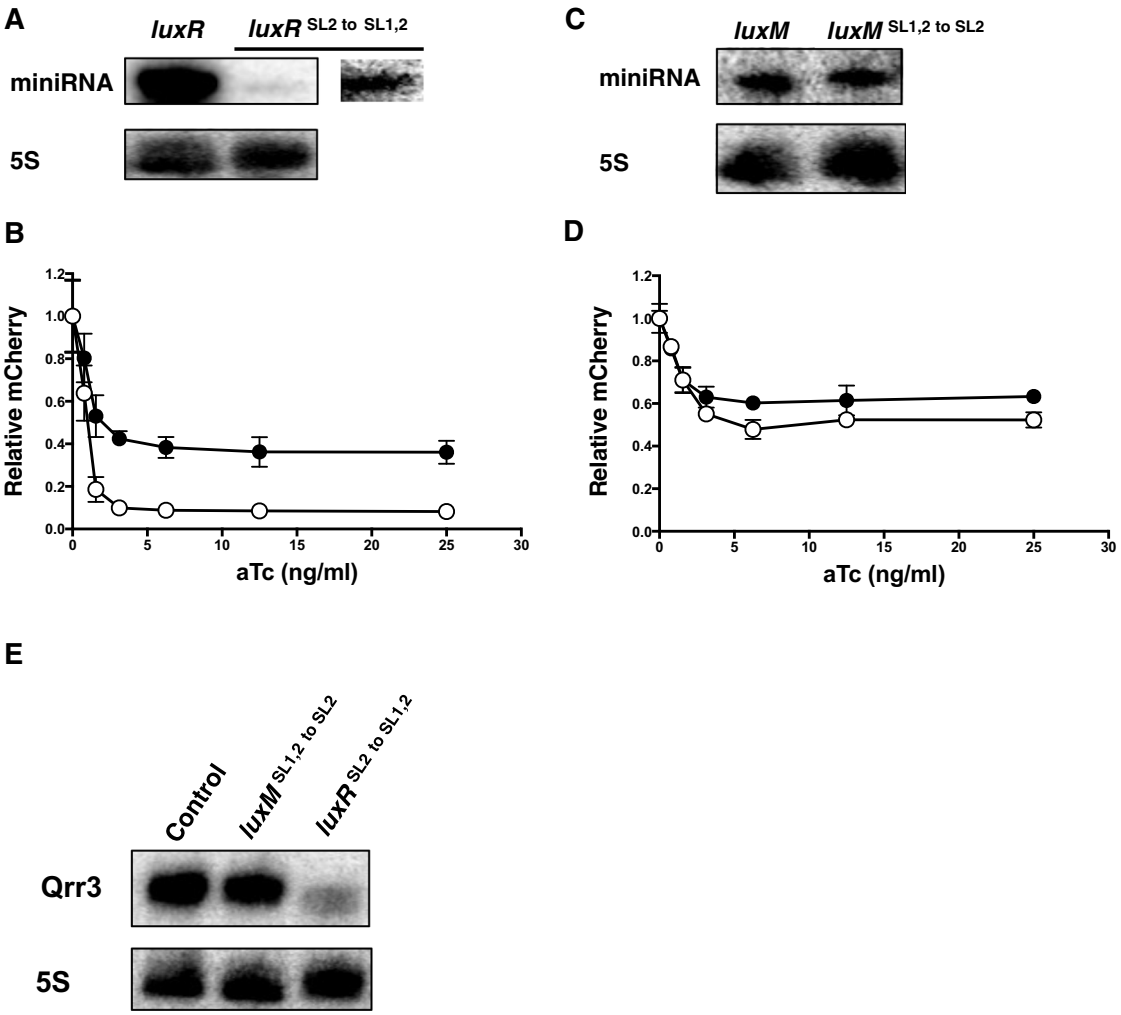

Figure S4. The miniRNAs Are Expressed and Regulated by Qrr3, Related to Figure 3

(A) Northern blots showing levels of the *luxR* miniRNA and the *luxR*$^{SL2\ to\ SL1,2}$ miniRNA. The contrast for the *luxR*$^{SL2\ to\ SL1,2}$ miniRNA signal was increased (right side of the miniRNA lane relative to that on the left side) in order to show its expression.

(B) Qrr3 regulation of *luxR* and *luxR*$^{SL2\ to\ SL1,2}$. Fluorescence was measured from *luxR-mCherry* (open circles) and *luxR*$^{SL2\ to\ SL1,2}$*-mCherry* (filled circles) translational fusions in the presence of the designated concentrations of anhydrotetracycline (aTc). aTc was used to induce Qrr3 expression from a plasmid. Data were normalized to that of the no aTc control. Means and SEMs for three cultures are shown.

(C) Northern blots showing levels of *luxM* miniRNA and *luxM*$^{SL1,2\ to\ SL2}$ miniRNA.

(D) Qrr3 regulation of *luxM* and *luxM*$^{SL1,2\ to\ SL2}$. Fluorescence was measured from *luxM-mCherry* (open circles) and *luxM*$^{SL1,2\ to\ SL2}$*-mCherry* (filled circles) translational fusions as in (B). Means and SEMs of three cultures are shown.

(E) Northern blot showing Qrr3 levels in the presence of the control, the *luxM*$^{SL1,2\ to\ SL2}$*-mCherry* mRNA or the *luxR*$^{SL2\ to\ SL1,2}$ *-mCherry* mRNA.

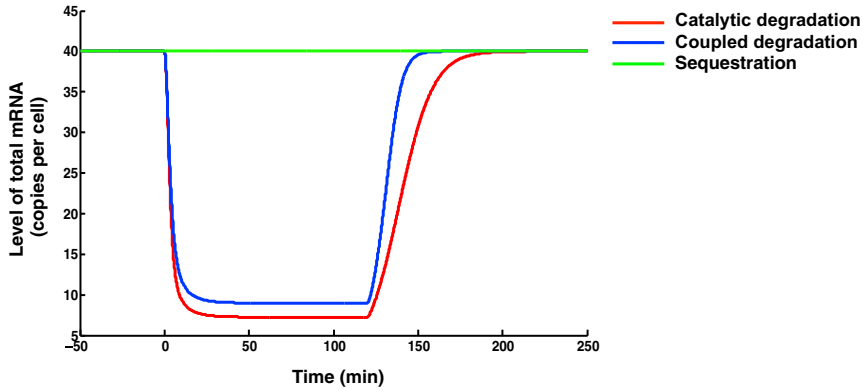

Figure S5. Dynamical Simulations for Total mRNA Levels when Different sRNA Regulatory Mechanisms Are Used, Related to Figure 6

The level of total mRNA is plotted over time based on Equations S1, S2, S3, S4, S5, and S6. sRNA production is induced at time zero and is terminated at 120 min. Three different regulatory mechanisms are shown: catalytic degradation (red), coupled degradation (blue), and sequestration (green).

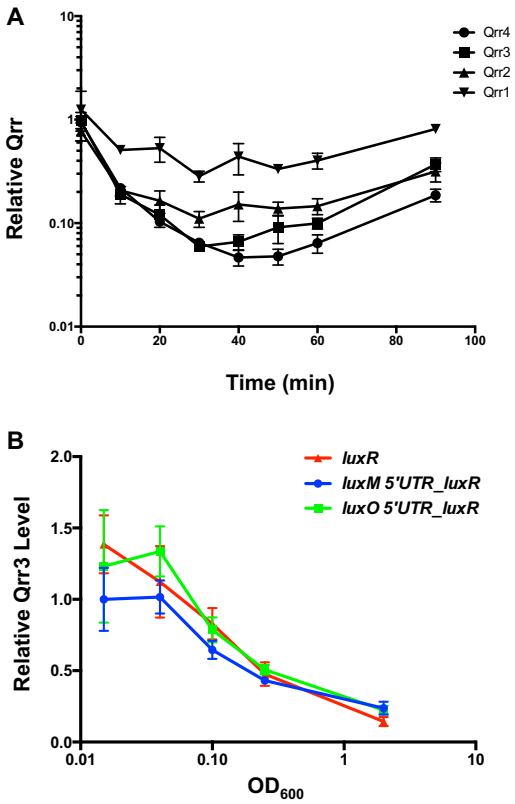

Figure S6. Particular Qrr Regulatory Mechanisms Are Crucial for Proper Quorum-Sensing Dynamics, Related to Figure 7

(A) Qrr1-4 were measured by qRT-PCR in *V. harveyi* strain TL25 following the addition of the autoinducer AI-1.

(B) Qrr3 was measured by qRT-PCR from *V. harveyi* strain LF2269 (Qrr3 only, *luxR* R17C) (red), LF2246 (Qrr3 only, *luxM* 5′UTR_*luxR* R17C) (blue), and LF2254 (Qrr3 only, *luxO* 5′UTR_*luxR* R17C) (green) as in Figure 7E. Data were normalized to the first 45 min time-point (OD_{600} = 0.015) of LF2246. Means and SEMs from four independent cultures are shown.

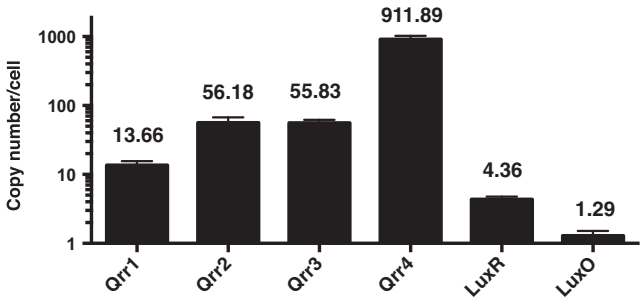

Figure S7. Copy Numbers of Qrr sRNAs and Target mRNAs in *V. harveyi*, Related to Figure 7

Copy numbers of Qrr1-4, *luxR* mRNA, and *luxO* mRNA in *V. harveyi* strain TL25 (a strain locked in low-cell-density mode) were measured as described in Extended Experimental Procedures. Means and SEMs from three independent cultures are shown.